RESPONSE CONTROL OF SEISMICALLY EXCITED BUILDINGS: APPLICATION OF VISCOUS DAMPING AND NEGATIVE STIFFNESS CONTROL ALGORITHM

A Thesis
Submitted to the Faculty
of
Purdue University
by
Huan Hu

In Partial Fulfillment of the
Requirements for the Degree
of
Master of Science

August, 2012
Purdue University
West Lafayette, Indiana

ACKNOWLEDGEMENTS

I would like to express my gratitude to my major advisor Dr. Shirley Dyke for accepting me as a graduate student under her supervision and helping with my research. Dr. Dyke has spent a lot of time in guiding my study and research, and provided me a lot of valuable advice and suggestions when I'm having difficult problems. Without her direction, this thesis would not have been completed.

Next, I would like to give thanks to my thesis committee members, Dr. Pujol and Dr. Rhoads, for their helps in the preparation of my thesis.

I would also like to thank my lab mates in IISL. They have not only provided me generous help and advice for my research and completion of the thesis, but also enriched the experiences in my life.

TABLE OF CONTENTS

Page

LIST OF TABLES v

LIST OF FIGURES vi

ABSTRACT viii

CHAPTER 1. INTRODUCTION 1

1.1. Structural Control 1

1.1.1. Passive Control 2

1.1.2. Active Control 3

1.1.3. Semi-active Control 4

1.2. Overview of Thesis 5

CHAPTER 2. LITERATURE REVIEW 6

2.1. Bouc-Wen MR Damper Model 6

2.2. H2/LQG Method 8

2.3. Clipping Algorithm 12

2.4. Pseudo Negative Stiffness Algorithm 14

CHAPTER 3. VISCOUS DAMPING AND NEGATIVE STIFFNESS CONTROL ALGORITHM 18

3.1. The Modal Model of Structure 18

3.1.1. Single Degree of Freedom 18

3.1.2. Multiple Degrees of Freedom 20

3.2. Structural Damping 24

3.2.1. Dynamic Magnification Factors 24

3.2.2. Response Reduction due to Increase of Damping 27

3.3. VDNS Control Strategy 28

3.4. Numerical Example: Response Control of Six-Story Building 31

3.5. Summary 37

CHAPTER 4. CASE STUDY: 20-STORY LINEAR BENCHMARK BUILDING 39

4.1. Benchmark Building Description 39

Page

4.2. Degradation Effects 42
4.3. Control System Design 44
4.3.1. Sensors 44
4.3.2. Control Devices 45
4.3.3. VDNS Controller 46
4.4. Evaluation Criteria 49
4.5. Numerical Results 52
4.5.1. Active Control System 52
4.5.2. Semi-Active Control System 54
4.6. Summary 67
CHAPTER 5. SUMMARY 70
5.1. Future Work 72
LIST OF REFERENCES 73

LIST OF TABLES

Table Page
Table 3.1: Parametric Study. 35
Table 3.2: Evaluation Criteria of Different Control Designs. 36
Table 4.1: Summary of Evaluation Criteria. 52
Table 4.2: Pre-Earthquake Evaluation Criteria for Active Control System. 62
Table 4.3: Post-Earthquake Evaluation Criteria for Active Control System. 63
Table 4.4: Pre-Earthquake Evaluation Criteria for Semi-Active Control System. 64
Table 4.5: Post-Earthquake Evaluation Criteria for Semi-Active System. 65
Table 4.6: Pre-Earthquake Evaluation Criteria for Sample Control System. 66
Table 4.7: Post-Earthquake Evaluation Criteria for Sample Control System. 67

LIST OF FIGURES

Figure Page
Figure 2.1: Bouc-Wen Model of MR Damper. 7
Figure 2.2: Graphical Representation of Clipped Optimal Control Algorithm. 13
Figure 2.3: Graphical Representation of Modified Clipped-Optimal Control. 14
Figure 2.4: Total Force at Bearing Location. 15
Figure 2.5: Simplified Model of the Cable-Stayed Bridge. 17
Figure 3.1: SDOF System. 19
Figure 3.2: 2-DOF System. 21
Figure 3.3: Dynamic Magnification Factor for Displacement. 26
Figure 3.4: Dynamic Magnification Factor for Acceleration. 27
Figure 3.5: Reduction of Dynamic Magnification Factor. 28
Figure 3.6: Schematic Diagram of Building with MR Dampers. 32
Figure 3.7: Simulink Model for Control System. 33
Figure 3.8: Relationship Between ζ and the Control Parameters k_d and c_d 35
Figure 3.9: Peak Responses of Each Floor of the Building. 37
Figure 4.1: Los Angeles 20-Story Building N-S MRF. 41
Figure 4.2: Node Numbers for the Los Angeles 20-Story Building N-S MRF. 42
Figure 4.3: Poles Locations of the Controlled Structure 50
Figure 4.4: Simulink Model for Control System. 51
Figure 4.5: Power Spectra of Earthquakes. 51
Figure 4.6: Comparison of Controlled and Uncontrolled Responses (Pre-Earthquake) 57
Figure 4.7: Comparison of Controlled and Uncontrolled Responses (Post-Earthquake). 58
Figure 4.8: Bar Chart Comparing the Evaluation Criteria for Pre-Earthquake Model. 59
Figure 4.9: Bar Chart Comparing the Evaluation Criteria for Post-Earthquake Model. 60

Figure Page

Figure 4.10: Ratios of Power Spectral Density Functions from Ground Acceleration to the First Floor Responses. 61

ABSTRACT

Hu, Huan. M.S.M.E., Purdue University, August 2012. Response Control of Seismically Excited Buildings: Application of Viscous Damping and Negative Stiffness Control Algorithm. Major Professor: Shirley J. Dyke, School of Mechanical Engineering.

This thesis focuses on the application of the viscous damping and negative stiffness (VDNS) algorithm to the seismic response control of buildings. It provides an effective option for the semi-active control of the earthquake excited buildings. The proposed VDNS control algorithm is a simple strategy, as compared to those control strategies requiring the designers to have deep understanding in modern control theory. It reduces the vibrations of the building by increasing the damping of the structure. The algorithm produces a control force that only requires measurements at the location of the control device. Therefore, the VDNS controller can be designed decentralized. The VDNS algorithm is evaluated on the numerical models of two buildings: a six-story building and a 20-story benchmark building. Active and semi-active control systems are designed based on the VDNS algorithm, to demonstrate its applications in both active and semi-active control. It is observed to be effective in reducing the responses of both buildings under earthquakes significantly.

CHAPTER 1. INTRODUCTION

Buildings around the world are subject to various loading conditions. During the design of a building, the designer must estimate the loads related to the building itself, for example the static forces due to connections. However, the building would also possibly be affected by external excitations, such as earthquakes. These disturbances induce undesired vibrations in the building, make people uncomfortable, cause damage to the structure and the equipment, and reduce the life of the building. Because the disturbances are dynamic in nature and highly uncertain with respect to magnitude and arrival times, the uncertainties make the design challenging at times. Based on the modern control theory, structural control has emerged to mitigate the negative effects that the external disturbances impose on the structures. Proposed originally by Yao [1], structural control has been investigated and shown great potential for reducing vibrations in various civil structures under dynamic loading. As compared to the traditional methods, for example the bracing systems, the structural control is more adaptable. Traditional methods are designed to remain the building in the elastic range. When the braces are selected far stronger than required, it might induce big accelerations in strong earthquakes. Serious efforts have been undertaken in the last three decades to develop the structural control concept into a workable technology.

1.1. Structural Control

The mitigation of structural vibrations can be done by a variety of methods, such as modifying the masses, rigidities, damping, or shape, and by providing passive or active resistant forces. Therefore, structural control is usually classified by its method, or the type of device used to impart the control force. The three classes of structural control

devices include passive, active, and semi-active, which correspond to passive, active and semi-active control respectively [2].

1.1.1. Passive Control

A passive control device is a device that produces a control force at the location of the device by using the motion of the structure, to limit the effects of seismic excitation. Because the system is purely reactive, the passive control device can only dissipate energy from the structure. This characteristic allows passive control to be considered as bounded input-bounded output (BIBO) stable. Furthermore, a passive control device does not require an external power supply. Passive control devices include auxiliary dampers, tuned mass dampers (TMD), and base isolation systems [3][4].

Auxiliary dampers have been successfully employed for flexible structures such as tall building, particularly those susceptible to strong winds. The damping devices, either viscous, viscoelastic, or plastic, utilize the flow of fluid to produce the resistant force to the structure, and dissipate energy. The World Trade Center in New York City and several buildings in Seattle and in California are employed with the auxiliary dampers [2][5].

A tuned mass damper is a classical dynamic vibration absorber, consisting of a mass on the order of 1% of the mass of the total structure, located at the top of the building and connected through a passive spring and damper. While this is a particularly effective strategy for stationary, narrow band motions, it is less for broadband excitations such as earthquakes, where transient effects are dominant [5]. However, the designer has several parameters, including mass ratio and absorber damping ratio, with which the bandwidth and attenuation capability of the device can be controlled. One of the world's tallest structures, the Taipei 101, employs a tuned mass damper to protect against the seismically active region of Taiwan [2][5]. Other examples are the John Hancock Tower in Boston and the Citicorp building in New York City [2][5].

In a structure with a base isolation system [6], the typical fixed-base design is replaced with an isolation system, such as elastomeric (rubber) bearings, between the base of the building and the ground. The effect of the base isolation system is to be stiff under vertical loads and at the same time flexible under lateral loads. Therefore, the result is that the base isolation system will reduce forces transmitted to the structure.

1.1.2. Active Control

One problem of passive control system is that the resistant forces provided by the passive control devices are not able to be controlled in a specified way. In order to compensate for the lack of adaptability of passive control devices, active control devices have been investigated and implemented. In an active control system, actuators are used to generate control forces to the structure. The force provided by the actuator can be controlled by adjusting the electrical input to the actuator to reduce the effects of external disturbances on the structure. Feedback measurements of the excitation and/or structural responses are used by an active control system to develop the required control forces. The structural responses are measured using sensors mounted at certain locations on the structure. Active control devices include active bracing systems, active mass damper (AMD) systems, and active base isolation systems [4]. Furthermore, a control algorithm uses the feedback measurements to determine the appropriate control forces to be applied to the structure. Control algorithms are being continually developed and improved to provide the most effective active control schemes.

Spencer et al. [7] provided a benchmark on a three-story building employing an active mass driver, and develop specifications and guidelines governing both performance and implementability for the evaluation of active structural control algorithms or the comparison between different control systems. The H2/LQG control law has been shown to be an effective control algorithm for active device for seismically excited structures [8]. Dyke et al. [9][10] investigated the use of acceleration feedback algorithms as opposed to

direct measurements of displacements and velocities which are impractical for full scale implementations.

Active control systems require external power supply to effect the control action. This makes such systems vulnerable to power failure, which is always a possibility during a strong earthquake. In addition, in contrast to a passive control device, an active control device can add energy to the structural system, thereby aggravating the effects of ground excitations.

1.1.3. Semi-active Control

A semi-active control device is a combination of passive and active control devices. On one hand, like passive control devices, semi-active control devices provide forces to the structure as a result of the response of the structure and would not add energy to the structure. Therefore, the semi-active control system is said to be reliable. On the other hand, feedback measurements are used by a controller to produce an appropriate signal for the semi-active control device, so the semi-active control system is adaptable, like the active control system. Furthermore, only a small external power source is required for the operation of a semi-active control device. Another attractive feature of semi-active control systems is that in the event of a power outage, the control system will revert to a passive system. As with active control, the performance of semi-active control is reliant on the ability of control algorithms implemented in the system. Examples of semi-active devices include variable orifice dampers, variable friction dampers, and magnetorheological dampers. These semi-active devices are implemented in the same manner as active control devices.

One challenge in the application of semi-active technology is in developing the nonlinear control algorithms that are appropriate for implementation in the structures. A number of control algorithms have been developed for semi-active systems. Leitmann designed a semi-active controller based on the Lyapunov stability theory [11]. The goal of this

algorithm is to reduce the responses by minimizing the rate of change of a Lyapunov function. McClamroch et al. developed a decentralized bangbang controller using a similar approach [12]. This control algorithm acts to minimize the total energy in the structure. Clipped-optimal controllers have also been proposed and implemented for semi-active systems. Jansen et al. [13] compared the performance of a number of semi-active control algorithms for use with multiple MR dampers to control a seismically excited building structure. It has been demonstrated that the performance of semi-active systems is highly dependent on the choice of control algorithm [18].

1.2. Overview of Thesis

This thesis focuses on the application of the viscous damping and negative stiffness (VDNS) control algorithm to the seismic response control of civil buildings. It provides an effective option for the semi-active control of the earthquake excited buildings. The H2/LQG control method and pseudo negative stiffness (PNS) algorithm are discussed in Chapter 2. The modeling of MR damper and the original and modified clipping algorithm for the semi-active control systems will be provided in Chapter 2 as well. Chapter 3 proposes the VDNS control algorithm which is designed to increase the damping of structure, and presents how this algorithm works on a six-story building. In Chapter 4, the VDNS algorithm is applied to the linear full scale 20-story benchmark building model. Two control systems are designed, and the results are discussed in this chapter. Finally, Chapter 5 summarizes the research and provides recommendations for future investigations.

CHAPTER 2. LITERATURE REVIEW

Control devices and strategies are continually being developed and studied to address different structural control issues and improve the performance of the control systems. In this chapter, the characteristics and modeling of a promising semi-active device, MR damper, are provided. The MR damper is used as the control device in the semi-active control systems in the later chapters in this thesis. The H2/LQG method and clipped-optimal controller are widely used control strategies for active and semi-active control systems respectively, and are discussed in detail in this chapter. A control algorithm using the pseudo negative stiffness (PNS) hysteretic loop for the seismic response control of cable-stayed bridges is also provided.

2.1. Bouc-Wen MR Damper Model

A particular semi-active device that has shown to be quite effective is the magneto-rheological (MR) damper. This device is a damper that contains a special fluid that has the reversible capacity to change from a Newtonian fluid to a semi-solid state that has a yield stress associated with it in a matter of milliseconds. The yield stress of the MR fluid is limited by a magnetic saturation, and is 50~100 kPa for an applied magnetic field of 150 ~250 kA/m. The fluid itself consists of some carrier medium such as hydrocarbon oil or silicone oil with micron-sized magnetically polarized particles dispersed in them. When this fluid is exposed to a magnetic field, the particles bond together, providing additional resistance due to the increased yield stress. The resultant control forces the dampers produce are dependent on the strength of the magnetic field applied.

Because the control forces are adjusted by the magnetic field and do not require a mechanical valve, the MR device displays high reliability. To produce these magnetic

fields, only 1 ~ 3 Amps and 20 ~ 60 Volts are usually needed. Thus, only a small power source, such as a battery, is required for the MR damper. Other advantages of MR damper are: 1. the performance is stable in a broad temperature range, e.g., MR fluid operates at temperature between -40 ^{o}C and 150 ^{o}C; 2. the response time is a few milliseconds; 3. the performance is not sensitive to contamination during manufacturing the MR damper; 4. it is relatively inexpensive to manufacture and maintain. The MR damper has also been experimentally validated for various types and capacities [23].

Accurate modeling of the MR damper's mechanical properties is necessary for predicting the behavior of the controlled system. Although, many models for the MR damper exist, this study employs the Bouc-Wen model. A schematic of a simple mechanical MR damper using the Bouc-Wen hysteresis model is shown in Figure 2.1. This particular model was developed and shown to accurately predict the behavior of the controlled system over a wide range of inputs in various experiments [19][20].

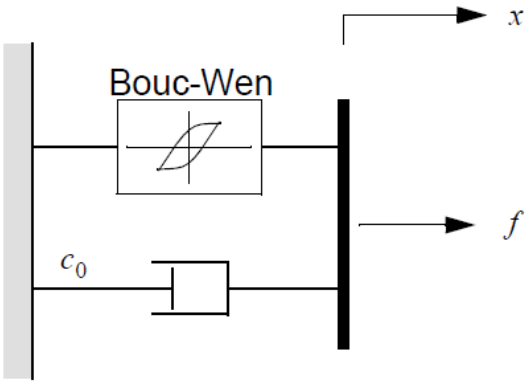

Figure 2.1: Bouc-Wen Model of MR Damper.

The equations governing the force produced by this device model are

$$f = c_0\dot{x} + \alpha z \tag{2.1}$$

$$\dot{z} = -\gamma|\dot{x}|z|z|^{n-1} - \beta\dot{x}|z|^{n} + A\dot{x} \tag{2.2}$$

where x is the displacement of the device, and z is an evolutionary variable that accounts for the history dependence of the response. By adjusting the parameters of the model γ, β, n, and A, the linearity in the unloading and smoothness of the transition from the pre-yield to the post-yield region can be controlled. The functional dependence of the device parameters on the command input u is modeled as

$$\alpha = \alpha_a + \alpha_b u \tag{2.3}$$

$$c_0 = c_{0a} + c_{0b} u. \tag{2.4}$$

The current driver circuit of the MR damper also introduces dynamics into the system. These dynamics are typically considered to be a first order time lag in the response of the devices to changes in the command input. These dynamics are accounted for with the first order filter on the control input given by

$$\dot{u} = -\eta(u - v) \tag{2.5}$$

where v is the command voltage applied to the control circuit.

2.2. H2/LQG Method

Consider a seismically excited structure controlled with n control devices. Assuming that the forces provided by the control devices are adequate to keep the response of the primary structure from exiting the linear region, the equations of motion can be written as

$$\mathbf{M}\ddot{\mathbf{x}} + \mathbf{C}\dot{\mathbf{x}} + \mathbf{K}\mathbf{x} = \Lambda\mathbf{f} - \mathbf{M}\Gamma\ddot{x}_g \tag{2.6}$$

where $\mathbf{M}$, $\mathbf{C}$, and $\mathbf{K}$ are the mass, damping and stiffness matrices of the structure, $\mathbf{x}$ is a vector of the relative displacements of the structure, Λ is a matrix determined by the placement of the control devices in the structure, $\mathbf{f} = [f_1, f_2, \ldots, f_n]^T$ is the vector of the measured control force provided by the *n* control devices, Γ is a column vector of ones, and $\ddot{x}_g$ is a one-dimensional ground acceleration.

The equations expressed above can be written in state-space form as

$$\dot{\mathbf{x}}_s = \mathbf{A}\mathbf{x}_s + \mathbf{B}\mathbf{f} + \mathbf{E}\ddot{x}_g \tag{2.7}$$

$$\mathbf{y}_m = \mathbf{C}_m\mathbf{x}_s + \mathbf{D}_m\mathbf{f} + \mathbf{F}_m\ddot{x}_g + \mathbf{v}_m \tag{2.8}$$

$$\mathbf{z} = \mathbf{C}_z\mathbf{x}_s + \mathbf{D}_z\mathbf{f} + \mathbf{F}_z\ddot{x}_g \tag{2.9}$$

where $\mathbf{x}_s$ is the state vector, $\mathbf{y}_m$ is the vector of measured outputs, $\mathbf{z}$ is the regulated output vector, $\mathbf{v}_m$ is a vector of measurement noises, and $\mathbf{A}$, $\mathbf{B}$, $\mathbf{E}$, $\mathbf{C}_m$, $\mathbf{D}_m$, $\mathbf{F}_m$, $\mathbf{C}_z$, $\mathbf{D}_z$, and $\mathbf{F}_z$ are matrices of appropriate dimension.

An H2/LQG control law has shown to be effective for structures affected by earthquake excitation [19], even in the case of nonlinear behavior [27][28]. In this approach, $\ddot{x}_g$ is taken as a stationary white noise, and an infinite horizon performance is chosen that weights the regulated output vector, $\mathbf{z}$, i.e.,

$$J = \lim_{\tau\to\infty}\frac{1}{\tau}\left[\int_0^{\tau}\left\{(\mathbf{C}_z\mathbf{x}_s + \mathbf{D}_z\mathbf{u})^T\mathbf{Q}(\mathbf{C}_z\mathbf{x}_s + \mathbf{D}_z\mathbf{u}) + \mathbf{u}^T\mathbf{R}\mathbf{u}\right\}dt\right] \tag{2.10}$$

where $\mathbf{R}$ is an identity matrix and the elements of the weighting matrix $\mathbf{Q}$ are selected to appropriately weight the regulated outputs. Further, the measurement noise is assumed to

be identically distributed, statistically independent Gaussian white noise processes, and $S_{\ddot{x}_g\ddot{x}_g} / S_{v_i v_i} = 25$.

The separation principle allows the control and estimation problems to be considered separately, yielding a controller of the form

$$\mathbf{u} = -\mathbf{K}\hat{\mathbf{x}}. \tag{2.11}$$

The matrix **K** is the optimal gain matrix for the Linear Quadratic Regulator (LQR) with full state feedback which is expressed in state-space form as

$$\mathbf{K} = \tilde{\mathbf{R}}^{-1}(\tilde{\mathbf{N}} + \mathbf{B}^T\mathbf{P}) \tag{2.12}$$

where **P** is the solution of the algebraic Riccati equation given by

$$\mathbf{P}\tilde{\mathbf{A}} + \tilde{\mathbf{A}}^T\mathbf{P} - \mathbf{P}\mathbf{B}\tilde{\mathbf{R}}^{-1}\mathbf{B}^T\mathbf{P} + \tilde{\mathbf{Q}} = \mathbf{0} \tag{2.13}$$

and

$$\tilde{\mathbf{Q}} = \mathbf{C}_z^T\mathbf{Q}\mathbf{C}_z - \tilde{\mathbf{N}}\tilde{\mathbf{R}}^{-1}\tilde{\mathbf{N}}^T \tag{2.14}$$

$$\tilde{\mathbf{N}} = \mathbf{C}_z^T\mathbf{Q}\mathbf{D}_z \tag{2.15}$$

$$\tilde{\mathbf{R}} = \mathbf{R} + \mathbf{D}_z^T\mathbf{Q}\mathbf{D}_z \tag{2.16}$$

$$\tilde{\mathbf{A}} = \mathbf{A} - \mathbf{B}\tilde{\mathbf{R}}^{-1}\tilde{\mathbf{N}}^T. \tag{2.17}$$

The solutions are detailed in [4][7]. The MATLAB routine *lqry.m* within the control toolbox can be used to calculate **K**.

In most real world problems, all the states are not available for measurement. Therefore, observer design techniques are developed to estimate the full state vector from only partial information developed from a measured outputs that capture enough information regarding the system dynamics. The vector $\hat{\mathbf{x}}$ is the estimated state vector using the Kalman filter

$$\dot{\hat{\mathbf{x}}} = \mathbf{A}\hat{\mathbf{x}} + \mathbf{B}\mathbf{u} + \mathbf{L}(\mathbf{y}_m - \mathbf{C}_m\hat{\mathbf{x}} - \mathbf{D}_m\mathbf{u}). \tag{2.18}$$

The matrix **L** is the observer gain matrix for the Linear Quadratic Gaussian (LQG) where

$$\mathbf{L} = \left[\underset{\sim}{\mathbf{R}}^{-1}(\gamma\mathbf{F}_m\mathbf{E}^T + \mathbf{C}_m\mathbf{S})\right]^T, \tag{2.19}$$

where **S** is the solution of the algebraic Riccati equation given by

$$\mathbf{S}\underset{\sim}{\mathbf{A}} + \underset{\sim}{\mathbf{A}}^T\mathbf{S} - \mathbf{S}\underset{\sim}{\mathbf{G}}\mathbf{S} + \underset{\sim}{\mathbf{H}} = \mathbf{0} \tag{2.20}$$

and

$$\underset{\sim}{\mathbf{A}} = \mathbf{A}^T - \mathbf{C}_m^T\underset{\sim}{\mathbf{R}}^{-1}(\gamma\mathbf{F}_m\mathbf{E}^T) \tag{2.21}$$

$$\underset{\sim}{\mathbf{G}} = \mathbf{C}_m^T\underset{\sim}{\mathbf{R}}^{-1}\mathbf{C}_m \tag{2.22}$$

$$\underset{\sim}{\mathbf{H}} = \gamma\mathbf{E}\mathbf{E}^T - \gamma^2\mathbf{E}\mathbf{F}_m^T\underset{\sim}{\mathbf{R}}^{-1}\mathbf{F}_m\mathbf{E}^T \tag{2.23}$$

$$\underset{\sim}{\mathbf{R}} = \mathbf{I} + \gamma\mathbf{F}_m\mathbf{F}_m^T. \tag{2.24}$$

The MATLAB routine *lqew.m* within the control toolbox can be used to calculate **L**.

The control force provided by each active control device is given by

$$f_i(t) = u_i(t) \tag{2.25}$$

where $u_i(t)$ is the ith command force determined by the control algorithm. In other words, the measured forces for the active control devices are the desired forces from the control algorithm.

2.3. Clipping Algorithm

Because the force generated in the MR damper is dependent on the local responses of the structural system, the desired control force f_{di} cannot always be produced by the MR damper. Only the control voltage V_i can be directly controlled to increase or decrease the force produced by the device. Thus, a force feedback loop is incorporated to induce the MR damper to generate approximately the desired control force f_{di}.

To induce the MR damper to generate approximately the desired control force, a clipping algorithm is needed for the MR damper to track the desired control force. In the original clipped optimal control algorithm [19][20], H2/LQG controllers described in Section 2.2 are first employed to determine the desired optimal control force. Then the clipping algorithm described following is used to select the command signal for the MR damper. When the *i*th MR damper is providing the desired control force (i.e., $f_i = f_{di}$), the voltage applied to the damper should remain at the present level. If the magnitude of the force produced by the damper is smaller than the magnitude of the desired control force and the two forces have the same sign, the voltage applied to the current driver is increased to the maximum level so as to increase the force produced by the damper to track the desired control force. Otherwise, the commanded voltage is set to zero. The algorithm for

selecting the command signal for the *i*th MR damper is graphically represented in Figure 2.2 and can be stated as

$$v_i = V_{max} H\left(\{f_{di} - f_i\} f_i\right) \tag{2.26}$$

where $V_{\max}$ is the maximum voltage to the current driver, and $H(\cdot)$ is the Heaviside step function.

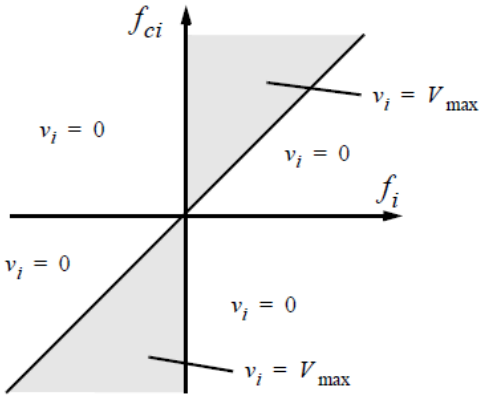

Figure 2.2: Graphical Representation of Clipped Optimal Control Algorithm [27].

In the original clipping algorithm, command voltage takes on values of either zero or the maximum value. The controller based on this algorithm would be classified as a bang-bang controller. In some situations, large changes in the forces applied to the structure may result in high local acceleration values. A modified version of this clipping algorithm was later proposed by Yoshida [27][28]. In this variation, the voltage can be any value between 0 and $V_{\max}$. The control voltage, denoted V_{ci}, is determined using a linear relationship between the applied voltage and the maximum force of MR. When the desired control force exceeds the maximum force of the MR damper, the maximum voltage is applied. The modified clipping is graphically represented in Figure 2.3 and can be stated as

$$v_i = V_{ci} H\left(\{f_{di} - f_i\} f_i\right) \tag{2.27}$$

where

$$V_{ci} = \begin{cases} \mu_i f_{di} & for\ f_{di} \le f_{\max} \\ V_{\max} & for\ f_{di} > f_{\max} \end{cases} \tag{2.28}$$

where $f_{\max}$ is the maximum force produced by the control device and μ_i is the coefficient relating the voltage to the force.

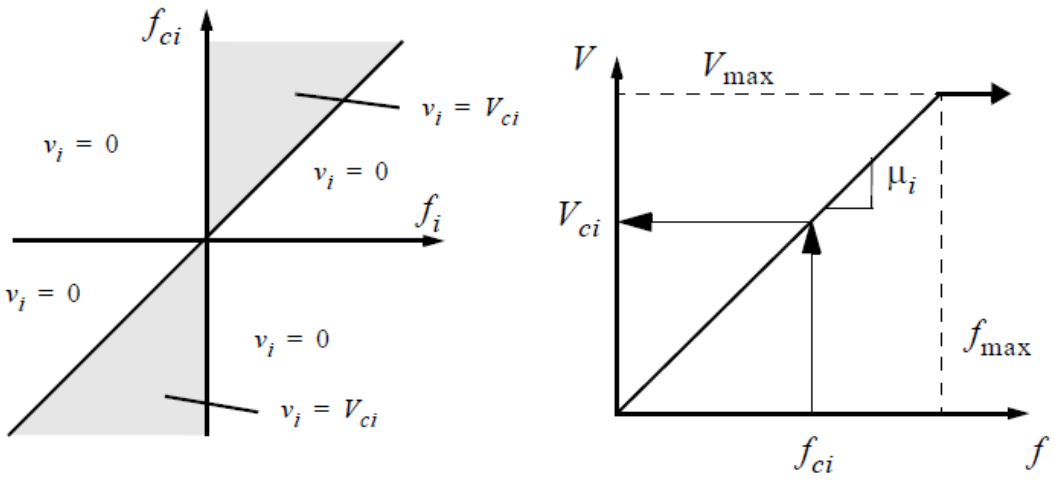

Figure 2.3: Graphical Representation of Modified Clipped-Optimal Control [27].

2.4. Pseudo Negative Stiffness Algorithm

Iemura et al. proposed a pseudo negative stiffness (PNS) algorithm for the seismic response control of cable-stayed bridges [29][30][31][32]. The strategy is to create a pseudo negative stiffness hysteretic loop. The combination of pseudo negative stiffness hysteretic loop plus connecting stiffness produces an artificial hysteretic loop that approaches rigid-perfectly plastic force-deformation characteristics which has large damping ratio.

The point is that the damper is usually set parallel to an existing member that has some stiffness. Viscous dampers, for example, have elliptical hysteretic loops (Figure 2.4b) when excited by sinusoidal excitations. Since the force transferred to other members is the summation of the damper and existing-member stiffness forces, then it is interesting to see Figure 2.4c, which is the summation of existing-member stiffness force and damper force. It is clear that the maximum forces in Figure 2.4c are larger than the maximum existing-member forces in Figure 2.4a.

On the other hand, by producing a pseudo negative stiffness (PNS) hysteretic loop (Figure 2.4e), the maximum force in Figure 2.4f is kept the same as the existing-member stiffness force (Figure 2.4d) while keeping large area inside the hysteretic loop.

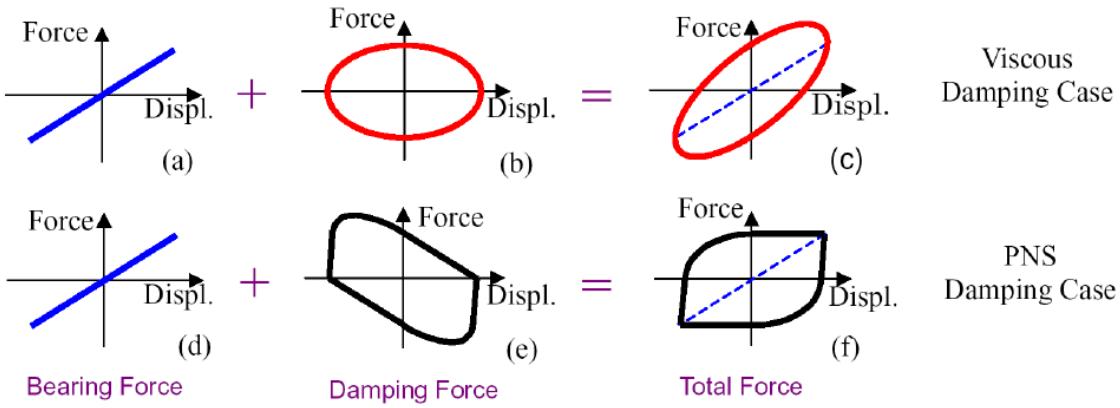

Figure 2.4: Total Force at Bearing Location [31].

An algorithm that can approach the hysteretic loop was proposed by Iemura et al. [29] as in Eq. (2.29)

$$f_d = k_d u + c_d \dot{u} \tag{2.29}$$

where k_d and c_d are selected negative stiffness and selected damping coefficient, respectively. The algorithm is practical because relative displacement and velocity sensors are located only at the variable dampers. The simple algorithm and relatively few sensors reduce the source of errors and uncertainties.

In order to study the effectiveness of this algorithm for seismic response control of cable-stayed bridges, applications of pseudo negative stiffness damper and linear viscous damper to the Tempozan bridge in Japan [29] and to the benchmark cable-stayed bridge in the US [30] were carried out using numerical simulations under several earthquake excitations. The results show that the pseudo negative stiffness damper reduces seismic responses better than those by passively viscous damper. The variable-orifice oil damper was used as the pseudo negative stiffness damper. By using this device, the opening ratio of the flow control can be changed by electric power based on a signal from the control PC. By changing it, the quantity of flow through the valve can be adjusted. This series of mechanism enables the variable damper to generate the force required as closely as possible.

To choose the values for the parameters of the pseudo negative stiffness damper, the cable-stayed bridge is simplified to a mass-spring system with only one mass as shown in Figure 2.5. The negative stiffness value k_d in Eq. (2.29) to control the variable damper is chosen as the negative value of the existing stiffness which is parallel to the damper. The damping coefficient c_d is selected by examining the effects of different values on the responses and induced forces of the bridge.

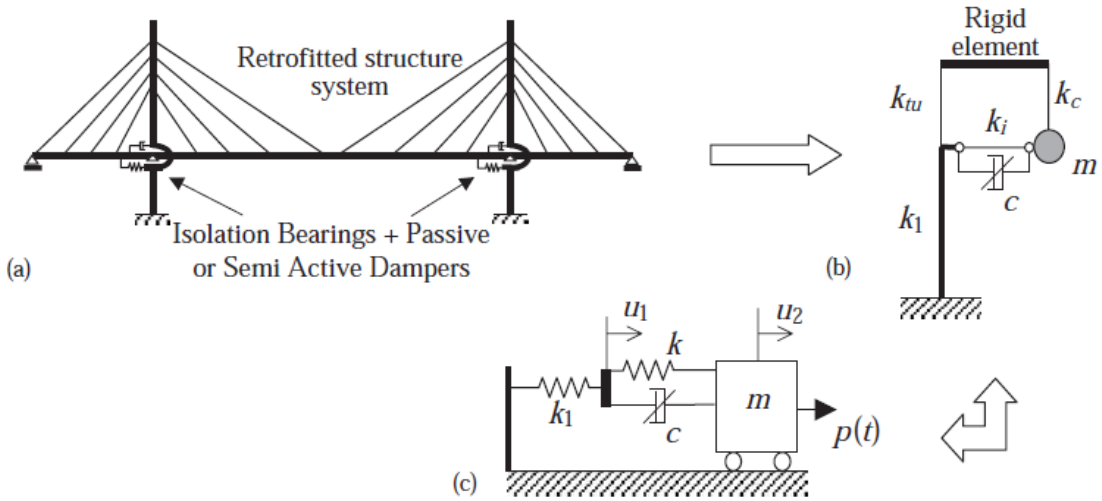

Figure 2.5: Simplified Model of the Cable-Stayed Bridge [29].

Iemura et al. also investigated the hysteretic loops produced by the LQR control force for seismic response, and reproduced the hysteretic loops with the proposed pseudo negative stiffness algorithm [32]. The results show that the proposed method is capable of reducing seismic response better than the viscous damper case and is similar to the LQR case. It needs only displacement response at the device location, and therefore fewer sensors are needed than for the LQR algorithm.

CHAPTER 3. VISCOUS DAMPING AND NEGATIVE STIFFNESS CONTROL ALGORITHM

In this chapter, a simple algorithm, viscous damping and negative stiffness (VDNS) algorithm, is provided for the response control of seismically excited buildings. This method was proposed by Weber et al. [36] for the mitigation of stay cable vibrations. The control force is designed to increase the damping of the structure, and it has the same form as that of the PNS algorithm. For a building usually with multiple degrees of freedom, it is convenient to study its modal model. The effects of the structural damping on the response of the structure are discussed in this chapter, and the first modal damping of the structure is used to determine the values of control parameters. The procedure of designing VDNS controller is demonstrated on a six-story building.

3.1. The Modal Model of Structure

Modes are inherent properties of a structure, and are determined by the material properties (mass, damping, and stiffness), and boundary conditions of the structure. Each mode is defined by a natural (modal or resonant) frequency, modal damping, and a mode shape (i.e. the so-called "modal parameters"). If either the material properties or the boundary conditions of a structure change, its modes will change. For instance, if mass is added to a structure, it will vibrate differently. To understand this, we will make use of the concept of single and multiple-degree-of-freedom systems.

3.1.1. Single Degree of Freedom

A single-degree-of-freedom (SDOF) system (see Figure 3.1 where the mass m can only move along the vertical x-axis) is described by the following equation

$$m\ddot{x}(t)+c\dot{x}(t)+kx(t)=f(t) \tag{3.1}$$

with m the mass, c the damping coefficient, and k the stiffness. The variable $x(t)$ stands for the position of the mass m with respect to its equilibrium point, i.e. the position of the mass when $f(t)\equiv 0$. Transforming Eq. (3.1) to the Laplace domain (assuming zero initial conditions) yields

$$Z(s)X(s)=F(s) \tag{3.2}$$

where $Z(s)$ is the dynamic stiffness

$$Z(s)=ms^2+cs+k. \tag{3.3}$$

The transfer function $H(s)$ between displacement and force, $X(s)=H(s)F(s)$, equals the inverse of the dynamic stiffness

$$H(s)=\frac{1}{ms^2+cs+k}. \tag{3.4}$$

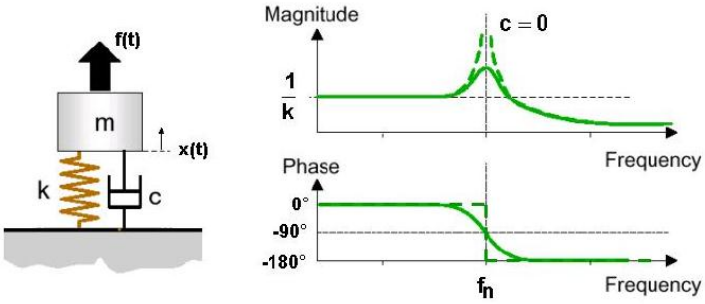

Figure 3.1: SDOF System.

The roots of the denominator of the transfer function, i.e. $d(s) = ms^2 + cs + k$, are the poles of the system. In most structures, the damping coefficient *c* is usually very small resulting in a complex conjugate pole pair

$$\lambda = -\sigma \pm i\omega_d. \tag{3.5}$$

ω_d is the damped natural frequency, $\omega_n = \sqrt{k/m} = |\lambda|$ is the (undamped) natural frequency, and $\zeta = c/2m\omega_n = \sigma/|\lambda|$ is the damping ratio ($\omega_d = \omega_n\sqrt{1-\zeta^2}$). If, for instance, a mass Δm is added to the original mass *m* of the structure, its natural frequency decreases to $\omega_n = \sqrt{k/(m+\Delta m)}$. If $c = 0$, the system is not damped and the poles becomes purely imaginary, $\lambda = \pm i\omega_n$.

The Frequency Response Function (FRF), denoted $H(\omega)$, is obtained by replacing the Laplace variable *s* in Eq. (3.4) by $i\omega$, resulting in

$$H(\omega) = \frac{1}{-m\omega^2 + ic\omega + k} = \frac{1}{(k - m\omega^2) + ic\omega}. \tag{3.6}$$

Clearly, if $c = 0$, then $H(\omega)$ goes to infinity as ω approaches to ω_n (See Figure 3.1).

Although very few practical structures could realistically be modeled by a single-degree-of-freedom (SDOF) system, the properties of such a system are important because those of a more complex multiple-degree-of-freedom (MDOF) system can always be represented as the linear superposition of a number of SDOF characteristics (when the system is linear time-invariant).

3.1.2. Multiple Degrees of Freedom

Multiple-degree-of-freedom (MDOF) systems are described by the following equation

$$\mathbf{M}\ddot{\mathbf{x}}(t)+\mathbf{C}\dot{\mathbf{x}}(t)+\mathbf{K}\mathbf{x}(t)=\mathbf{f}(t). \tag{3.7}$$

In Figure 3.2, the different matrices are defined for a 2-DOF system with both DOF along the vertical x-axis.

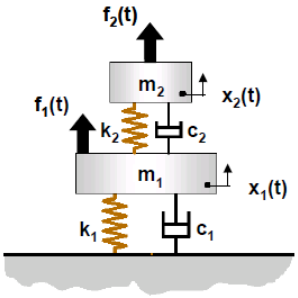

$$\mathbf{M}=\begin{bmatrix} m_1 & 0 \\ 0 & m_2 \end{bmatrix} \qquad \mathbf{f}(t)=\begin{Bmatrix} f_1(t) \\ f_2(t) \end{Bmatrix}$$

$$\mathbf{K}=\begin{bmatrix} k_1+k_2 & -k_2 \\ -k_2 & k_2 \end{bmatrix} \qquad \mathbf{x}(t)=\begin{Bmatrix} x_1(t) \\ x_2(t) \end{Bmatrix}$$

$$\mathbf{C}=\begin{bmatrix} c_1+c_2 & -c_2 \\ -c_2 & c_2 \end{bmatrix}$$

Figure 3.2: 2-DOF System.

Transforming Eq. (3.7) to the Laplace domain (assuming zero initial conditions) yields

$$\mathbf{Z}(s)\mathbf{X}(s)=\mathbf{F}(s) \tag{3.8}$$

where $\mathbf{Z}(s)$ is the dynamic stiffness matrix

$$\mathbf{Z}(s)=\mathbf{M}s^2+\mathbf{C}s+\mathbf{K}. \tag{3.9}$$

The transfer function matrix $\mathbf{H}(s)$ between displacement and force vectors, $\mathbf{X}(s)=\mathbf{H}(s)\mathbf{F}(s)$, equals the inverse of the dynamic stiffness matrix

$$\mathbf{H}(\mathbf{s})=\left[\mathbf{M}s^2+\mathbf{C}s+\mathbf{K}\right]^{-1}=\frac{\mathbf{N}(s)}{d(s)} \tag{3.10}$$

with the numerator polynomial matrix $\mathbf{N}(s)$ given by

$$\mathbf{N}(s) = \mathbf{adj}(\mathbf{M}s^2 + \mathbf{C}s + \mathbf{K}) \tag{3.11}$$

and the common denominator polynomial $d(s)$, also known as the characteristic polynomial,

$$d(s) = \det(\mathbf{M}s^2 + \mathbf{C}s + \mathbf{K}). \tag{3.12}$$

When the damping is small, the roots of the characteristic polynomial $d(s)$ are complex conjugate pole pairs, λ_m and λ_m^*, $m = 1, \ldots, N_m$, with N_m the number of modes of the system. The transfer function can be rewritten in a pole-residue form, i.e. the so-called "modal" model

$$\mathbf{H}(s) = \sum_{m=1}^{N_m} \frac{\mathbf{R}_m}{s - \lambda_m} + \frac{\mathbf{R}_m^*}{s - \lambda_m^*}. \tag{3.13}$$

The residue matrices $\mathbf{R}_m$, $m = 1, \ldots, N_m$ are defined by

$$\mathbf{R}_m = \lim_{s \to \lambda_m} \mathbf{H}(s)(s - \lambda_m). \tag{3.14}$$

It can be shown that the matrix $\mathbf{R}_m$ is of rank one meaning that $\mathbf{R}_m$ can be decomposed as

$$\mathbf{R}_m = \Psi_m \Psi_m^T = \begin{Bmatrix} \psi_m(1) \\ \psi_m(2) \\ \vdots \\ \psi_m(N_m) \end{Bmatrix} \begin{bmatrix} \psi_m(1) & \psi_m(2) & \cdots & \psi_m(N_m) \end{bmatrix} \tag{3.15}$$

with Ψ_m a vector representing the "mode shape" of mode *m*. From Eq. (3.13), one concludes that the transfer function matrix of a linear time-invariant MDOF system with N_m DOFs is the sum of N_m SDOF transfer functions ("modal superposition") and that the full transfer function matrix is completely characterized by the modal parameters, i.e. the poles $\lambda_m = -\sigma_m \pm i\omega_{d,m}$ and the mode shape vectors Ψ_m, $m = 1,\ldots,N_m$.

Taking the inverse Laplace transform of Eq. (3.13) yields the Impulse Response Function (IRF)

$$\mathbf{h}(t) = \sum_{m=1}^{N_m} \mathbf{R}_m e^{\lambda_m t} + \mathbf{R}_m^* e^{\lambda_m^* t} \tag{3.16}$$

which consists of a sum of complex exponential functions.

Eq. (3.7) can be written as

$$\dot{\mathbf{x}}_s(t) = \mathbf{A}x_s(t) + \mathbf{B}\mathbf{f}(t) \tag{3.17}$$

where $\mathbf{x}_s$ is the state vector, **A** and **B** are the state matrix and input matrix respectively, given by

$$\mathbf{A} = \begin{bmatrix} \mathbf{0} & \mathbf{I} \\ -\mathbf{M}^{-1}\mathbf{K} & -\mathbf{M}^{-1}\mathbf{C} \end{bmatrix} \tag{3.18}$$

$$\mathbf{B} = \begin{bmatrix} \mathbf{0} \\ \mathbf{M}^{-1} \end{bmatrix}. \tag{3.19}$$

The poles $\lambda_m = -\sigma_m \pm i\omega_{d,m}$ and the mode shape vectors Ψ_m ($m = 1,\ldots,N_m$) of the system can be determined by calculating the eigenvalues and eigenvectors of the state matrix **A**.

The MATLAB routine *eig.m* within the control toolbox can be used to calculate the eigenvalues and eigenvectors.

3.2. Structural Damping

Iemura et al. have shown that the pseudo negative stiffness (PNS) hysteretic loops can be produced by adding negative stiffness force to the viscous damping force [29][30][31]. By producing such PNS hysteretic loops, the maximum force is kept the same with existing-member stiffness forces while keeping large area inside the hysteretic loops. The effectiveness of this algorithm has been evaluated on a typical cable-stayed bridge in Japan and to the benchmark cable-stayed bridge in the US using numerical simulations under several earthquake excitations. The results show that the algorithm reduces displacement and keeps the base shear small in both cable-stayed bridges. Rather than considering the PNS hysteretic loops, the effect of the negative stiffness force on the structural damping is investigated in the thesis.

3.2.1. Dynamic Magnification Factors

Letting $f(t) = f_0 \sin(\omega t)$, where f_0 and ω are, respectively, the amplitude and the driving frequency of the forcing function; from Eq. (3.6), the steady-state response amplitude x_0 is given by

$$x_0 = \frac{f_0 / m}{\sqrt{\left(\omega_n^2 - \omega^2\right)^2 + \left(2\zeta\omega_n\omega\right)^2}} = \frac{f_0 / k}{\sqrt{\left(1 - \frac{\omega^2}{\omega_n^2}\right)^2 + \left(2\zeta\frac{\omega}{\omega_n}\right)^2}}. \tag{3.20}$$

Denoting the term multiplying f_0 / k on the right side of Eq. (3.20) by β_d results in

$$\beta_d = \frac{1}{\sqrt{\left(1-\frac{\omega^2}{\omega_n^2}\right)^2 + \left(2\zeta\frac{\omega}{\omega_n}\right)^2}} = \frac{f_0/k}{\sqrt{\left(1-r^2\right)^2 + \left(2\zeta r\right)^2}}. \tag{3.21}$$

Here, *r* is the frequency ratio with

$$r = \frac{\omega}{\omega_n}. \tag{3.22}$$

Therefore, the amplitude x_0 can be rewritten as

$$x_0 = \beta_d \frac{f_0}{k}. \tag{3.23}$$

In Eq. (3.23), the term f_0/k can be seen as a static displacement. That is, the amplitude of the dynamic displacement $x(t)$, namely, x_0, can be seen as the static displacement times a special factor β_d, which is referred to as the dynamic magnification factor for the displacement [38].

Figure 3.3 shows a set of curves of the dynamic magnification factors of displacement with different damping ratios. Figure 3.3 shows that the dynamics magnification factors β_d can be either larger or smaller than unity. When the frequency ratio is close to 1, the underdamped system will always have the value of β_d greater than unity. This phenomenon is defined as resonance. The smaller the damping, the larger the value of β_d found when resonance occurs. Pure resonant behavior occurs for an ideal system with zero damping; in which case, the response becomes limitless. When the damping ratio becomes larger than 0.707, the value of β_d will never be larger than unity. Furthermore, when the damping ratio is greater than 1, the system is overdamped.

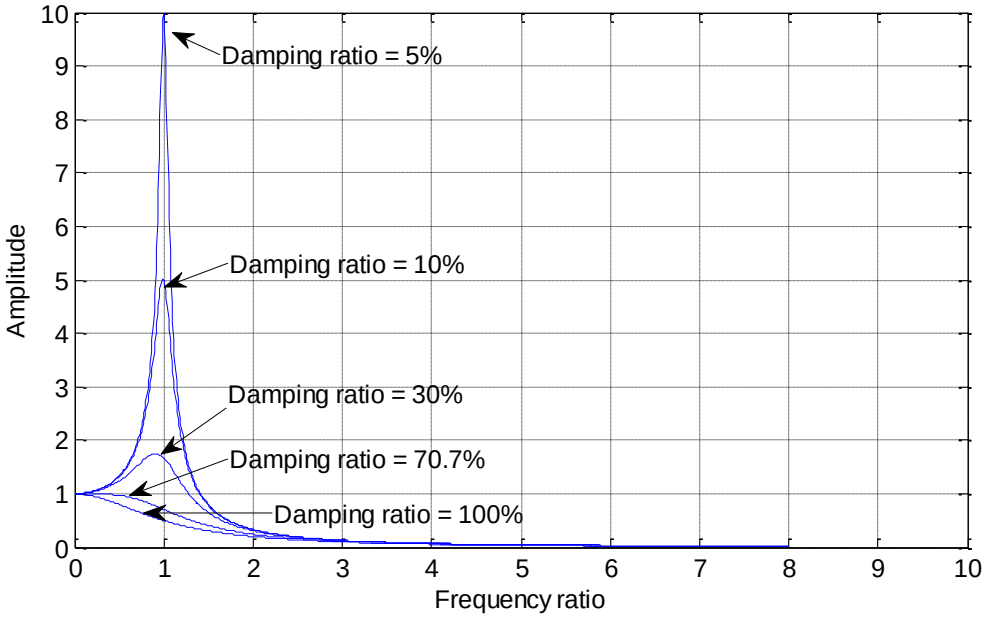

Figure 3.3: Dynamic Magnification Factor for Displacement.

The acceleration amplitude of steady-state response, denoted by a_0, can be written as

$$a_0 = \omega^2 x_0 = \frac{f_0}{k}\left[\frac{\omega^2}{\sqrt{\left(1-\frac{\omega^2}{\omega_n^2}\right)^2+\left(2\zeta\frac{\omega}{\omega_n}\right)^2}}\right] = \frac{f_0}{m}\left[\frac{\frac{\omega^2}{\omega_n^2}}{\sqrt{\left(1-\frac{\omega^2}{\omega_n^2}\right)^2+\left(2\zeta\frac{\omega}{\omega_n}\right)^2}}\right]. \quad (3.24)$$

The terms in the bracket on the right side of Eq. (3.24) can be denoted by β_a, as

$$\beta_a = \frac{\frac{\omega^2}{\omega_n^2}}{\sqrt{\left(1-\frac{\omega^2}{\omega_n^2}\right)^2+\left(2\zeta\frac{\omega}{\omega_n}\right)^2}} = \frac{r^2}{\sqrt{\left(1-r^2\right)^2+\left(2\zeta r\right)^2}}. \quad (3.25)$$

Here β_a is referred to as the dynamic magnification for the acceleration, which is shown in Figure 3.4.

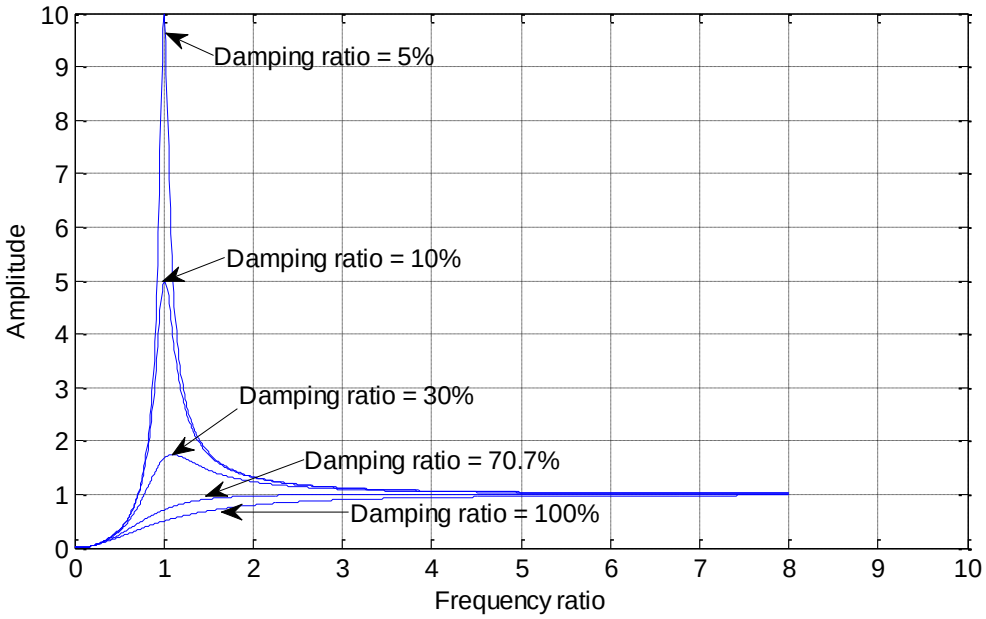

Figure 3.4: Dynamic Magnification Factor for Acceleration.

3.2.2. Response Reduction due to Increase of Damping

By examining both the dynamic magnification factors of the displacement and the acceleration, it is observed that when the damping ratio is increased, the vibration response can be reduced.

In Figure 3.5, several curves are plotted to compare the response reduction with the increased damping ratio at different frequency points. These curves, denoted by $R(\zeta)$, are percentage reduction, namely, the values of the Y-axis are

$$R(\zeta) = \frac{100\left[\beta_d(\zeta, r) - \beta_d(0.01, r)\right]}{\beta_d(0.01, r)} \tag{3.26}$$

and the X-axis is 100ζ. In Figure 3.5, the frequency ratios are chosen to be 1.5, 1.2, 1.1, 1.05, and 1. The corresponding curves are plotted and marked with these frequency ratios. It can be proven that the reduction curves of r = 1.5 and r = 1/1.5 are identical, and so on. In the resonant region around r = 1, the percentage reduction increases rapidly as the damping ratio increases. It is realized that increasing the damping ratio to reduce the displacement can be more effective in the resonant region.

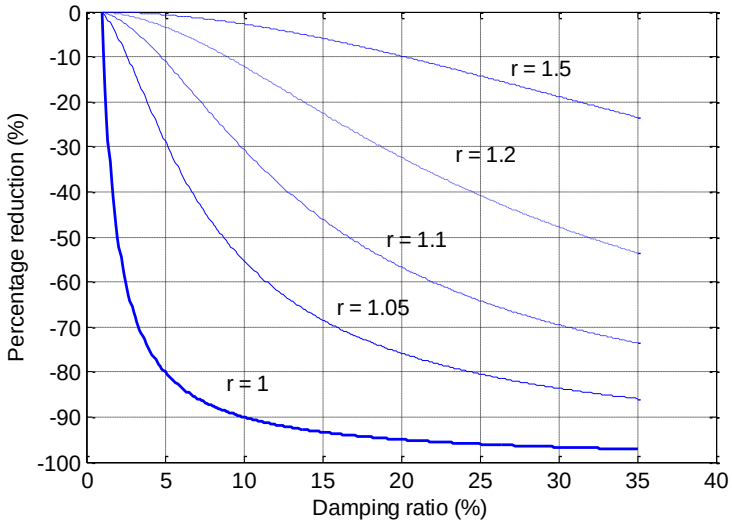

Figure 3.5: Reduction of Dynamic Magnification Factor.

3.3. VDNS Control Strategy

In this section, the procedure of the VDNS algorithm is provided. Consider a seismically excited structure controlled with n control devices. Assuming that the forces provided by the control devices are adequate to keep the response of the primary structure from exiting the linear region, the equations of motion can be written as

$$\mathbf{M}\ddot{\mathbf{x}} + \mathbf{C}\dot{\mathbf{x}} + \mathbf{K}\mathbf{x} = \Lambda\mathbf{f} - \mathbf{M}\Gamma\ddot{x}_g \tag{3.27}$$

where **x** is a vector of the relative displacements of the floors of the structure, $\ddot{x}_g$ is a one-dimensional ground acceleration, $\mathbf{f} = [f_1, f_2, \ldots, f_n]^T$ is the vector of measured control forces, Γ is a column vector of ones, and Λ is a vector determined by the placement of the control device in the structure. This equation can be written in state-space form as

$$\dot{\mathbf{x}}_s = \mathbf{A}\mathbf{x}_s + \mathbf{B}\mathbf{f} + \mathbf{E}\ddot{x}_g \tag{3.28}$$

$$\mathbf{y}_m = \mathbf{C}_m\mathbf{x}_s + \mathbf{D}_m\mathbf{f} + \mathbf{F}_m\ddot{x}_g + \mathbf{v}_m \tag{3.29}$$

$$\mathbf{z} = \mathbf{C}_z\mathbf{x}_s + \mathbf{D}_z\mathbf{f} \tag{3.30}$$

where $\mathbf{y}_m$ is the vector corresponding to measured outputs, $\mathbf{v}_m$ is a measurement noise vector, and **A**, **B**, **E**, $\mathbf{C}_m$, $\mathbf{D}_m$, and $\mathbf{F}_m$ are matrices of appropriate dimension. **z** is a vector of the horizontal displacements and velocities of those floors with control devices implemented relative to the ground.

The Viscous Damping and Negative Stiffness (VDNS) algorithm is to add the negative stiffness force to the viscous damping force, which calculates the desired control forces of the control devices based on the displacement and velocity of the devices, i.e., the desired control force of a control device f_{di} is given as

$$f_{di} = k_{di}d_i + c_{di}v_i \tag{3.31}$$

where d_i and v_i are the relative displacement and velocity across the *i*th control device, k_{di} is the negative stiffness coefficient, which has to be negative, and c_{di} is the damping coefficient, which has to be positive. Let all desired control forces have the same value of k_d and c_d, therefore, the vector of control force **f** can be written as

$$\mathbf{f}=\begin{Bmatrix} f_1 \\ f_2 \\ \vdots \\ f_n \end{Bmatrix}=\begin{Bmatrix} k_d x_{N_1}+c_d \dot{x}_{N_1} \\ k_d(x_{N_2}-x_{N_1})+c_d(\dot{x}_{N_2}-\dot{x}_{N_1}) \\ \vdots \\ k_d(x_{N_n}-x_{N_{n-1}})+c_d(\dot{x}_{N_n}-\dot{x}_{N_{n-1}}) \end{Bmatrix}=\mathbf{Tz} \tag{3.32}$$

where $\mathbf{T}=\begin{bmatrix}\mathbf{K}_d & \mathbf{C}_d\end{bmatrix}$ consists of the negative stiffness matrix $\mathbf{K}_d$ and the control damping matrix $\mathbf{C}_d$, and

$$\mathbf{K}_d=\begin{bmatrix} k_d & 0 & \cdots & 0 & 0 \\ -k_d & k_d & & 0 & 0 \\ \vdots & & \ddots & \vdots & \\ 0 & 0 & & k_d & 0 \\ 0 & 0 & \cdots & -k_d & k_d \end{bmatrix} \tag{3.33}$$

$$\mathbf{C}_d=\begin{bmatrix} c_d & 0 & \cdots & 0 & 0 \\ -c_d & c_d & & 0 & 0 \\ \vdots & & \ddots & \vdots & \\ 0 & 0 & & c_d & 0 \\ 0 & 0 & \cdots & -c_d & c_d \end{bmatrix}. \tag{3.34}$$

Using Eq. (4.5) in Eq. (4.7),

$$\mathbf{f}=\mathbf{Tz}=\mathbf{T}\left(\mathbf{C}_z\mathbf{x}_s+\mathbf{D}_s\mathbf{f}\right). \tag{3.35}$$

Therefore,

$$\mathbf{f}=\left(\mathbf{I}-\mathbf{TD}_z\right)^{-1}\mathbf{TC}_z\mathbf{x}_s. \tag{3.36}$$

Using Eq. (4.11) in Eq. (4.2), the controlled system becomes

$$\dot{\mathbf{x}}_s = \mathbf{A}_c \mathbf{x}_s + \mathbf{E}_c \ddot{x}_g \tag{3.37}$$

where

$$\mathbf{A}_c = \mathbf{A} + \mathbf{B}\left(\mathbf{I} - \mathbf{T}\mathbf{D}_z\right)^{-1} \mathbf{T}\mathbf{C}_z. \tag{3.38}$$

In most cases, $\mathbf{D}_z = \mathbf{0}$. The poles $\lambda_m = -\sigma_m \pm i\omega_{d,m}$ of the controlled system can be determined by calculating the eigenvalues of the state matrix $\mathbf{A}_c$. To ensure that the controlled system is stable, all eigenvalues of $\mathbf{A}_c$ must have negative real parts, i.e., $\sigma_m > 0$. The damping ratio of the first mode of the controlled structure ζ_1 can be calculated as

$$\zeta_1 = \frac{\sigma_1}{\omega_{n,1}} = \frac{\sigma_1}{\sqrt{\sigma_1^2 + \omega_{d,1}^2}}. \tag{3.39}$$

Finally, the control parameters k_d and c_d are selected to increase the value of ζ_1.

3.4. Numerical Example: Response Control of Six-Story Building

An example of how the VDNS algorithm works is illustrated on the numerical model of a six-story building that is controlled with four MR dampers. This building has been studied by Jansen et al. [13]. Two devices are rigidly connected between the ground and the first floor, and two devices are rigidly connected between the first and second floors, as shown in Figure 3.6. Each MR damper is capable of producing a force equal to 1.8% the weight of the entire structure, and the maximum voltage input to the MR devices is V_{max} = 5 V. The governing equations can be written in the form of Eq. (3.27) by defining the mass of each floor, m_i, as 0.227 N/(cm/sec2) (0.129 1b/(in/sec2)), the stiffness of each floor, k_i, as 297 N/cm (169 lb/in), and a damping ratio for each mode of 0.5%.

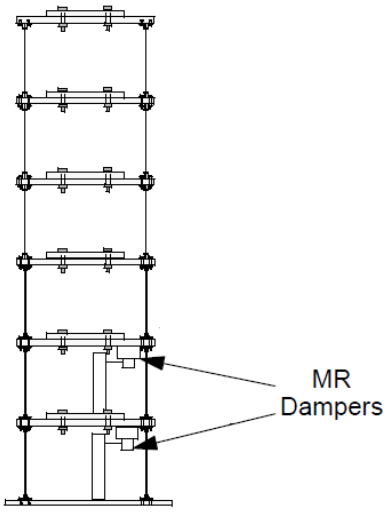

Figure 3.6: Schematic Diagram of Building with MR Dampers.

The Bouc-Wen model for the MR damper was presented in Chapter 2. The MR damper parameters used in this study are c_{0a} = 0.0064 N-sec/cm, c_{0b} = 0.0052 N-sec/cm-V, α_a = 8.66 N/cm, α_b = 8.66 N/cmV, γ = 300 cm^{-2}, γ = 300 cm^{-2}, A = 200, and n = 2. These parameters were selected based on the identified model of the shear-mode prototype MR damper.

In simulation, the model of the structure is subjected to the NS component of the 1940 El Centro earthquake. The simulations were performed in MATLAB. The Simulink model of the simulation is shown in Figure 3.7. The Runge-Kutta method is employed as the integrator and the integration time step is 0.0001 sec. Because the building system considered is a scaled model, the amplitude of the earthquake was scaled to ten percent of the full-scale earthquake to represent the magnitude of displacements that would be observed in laboratory experiments with this structure.

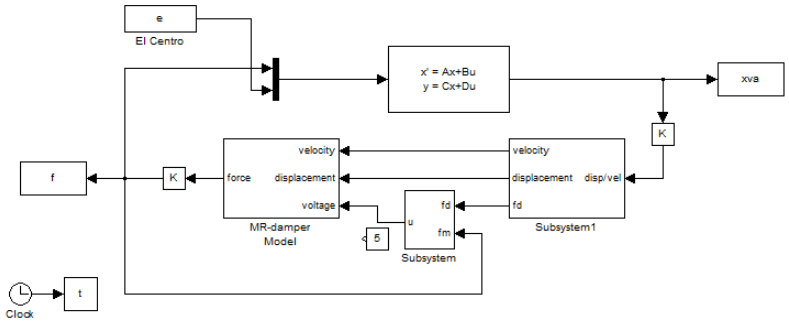

Figure 3.7: Simulink Model for Control System.

Four evaluation criteria are defined as following to evaluate and compare the control algorithms [13]. The first evaluation criterion is a measure of the normalized maximum floor displacement relative to the ground, given as

$$J_1 = \max_{t,i}\left(\frac{\left|x_i(t)\right|}{x^{max}}\right) \tag{3.40}$$

where $x_i(t)$ is the relative displacement of the *i*th floor over the entire response, and $x^{\max}$ denotes the uncontrolled maximum displacement. The second evaluation criterion is a measure of the reduction in the interstory drift. The maximum of the normalized interstory drift is

$$J_2 = \max_{t,i}\left(\frac{\left|d_i(t)/h_i\right|}{d_n^{max}}\right) \tag{3.41}$$

where h_i is the height of each floor (30 cm), $d_i(t)$ is the interstory drift of the above ground floors over the response history, and $d_n^{\max}$ denotes the normalized peak interstory drift in the uncontrolled response. The third evaluation criterion is a measure of the normalized peak floor accelerations, given by

$$J_3 = \max_{t,i}\left(\frac{\left|\ddot{x}_{ai}(t)\right|}{\ddot{x}_a^{max}}\right) \tag{3.42}$$

where the absolute accelerations of the ith floor, $\ddot{x}_{ai}(t)$, are normalized by the peak uncontrolled floor acceleration, denoted $\ddot{x}_a^{\max}$. The final evaluation criteria considered in this study is a measure of the maximum control force per device, normalized by the weight of the structure, given by

$$J_4 = \max_{t,i}\left(\frac{\left|f_i(t)\right|}{W}\right) \tag{3.43}$$

where W is the total weight of the structure (1335 N). The corresponding uncontrolled responses are as follows: $x^{\max}$ = 1.313 cm, $d_n^{\max}$ = 0.00981 cm, $\ddot{x}_a^{\max}$ = 146.95 cm/sec^2 [13].

Figure 3.8 shows the relationship between the structural damping ratio ζ and the control parameters k_d and c_d. In Figure 3.8, the absolute value of k_d is increased from 0 to 240 N/cm. As $|k_d|$ increases, the controlled structural damping ratio ζ is increased. For relative small value of $|k_d|$ ($|k_d|$<160 N/cm), ζ increases first with c_d increasing, and comes to the peak at certain point c_{d0}, and then start decreasing when c_d continues increasing. When k_d has a relative big absolute value, for example, $k_d = -240$ N/cm, ζ increases rapidly to 1 as c_d increases, which means the poles corresponding to the first mode of the controlled structure become closer and closer to the real axis in the complex plane. When the value of c_d continues to increase, the poles are observed to start crossing into the right half plane (RHP), and the control system becomes unstable.

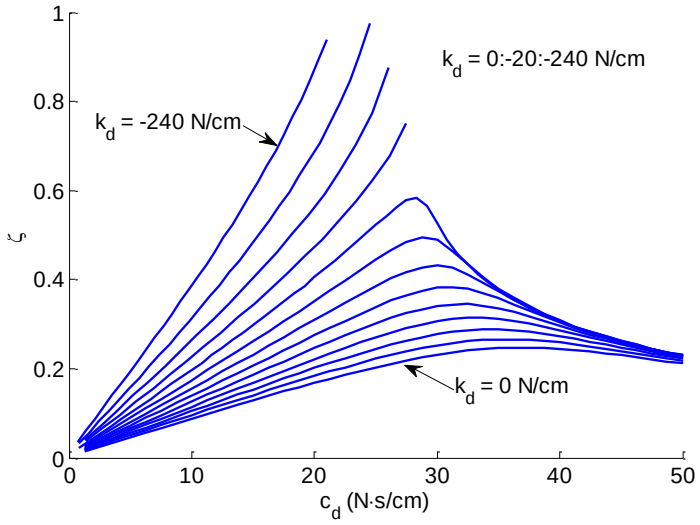

Figure 3.8: Relationship Between ζ and the Control Parameters k_d and c_d.

Figure 3.8 is used to guide the selection of the values of control parameters. Because the force generated by the MR damper is dependent on the local responses of the structural system, the desired control force cannot always be produced by the MR damper. Thus, the original clipping algorithm discussed in Section 2.3 is used to induce the MR damper to generate approximately the desired control force. Parametric study is conducted for the control system with various values of control parameters k_d and c_d. The results are given in Table 3.1.

Table 3.1: Parametric Study.

Coefficients	J_1	J_2	J_3	J_4
$k_d = 0$, $c_d = 37$	0.546 (+8%)	0.630 (-9%)	0.566 (-37%)	0.0174
$k_d = -40$, $c_d = 35$	0.529 (+5%)	0.601 (-14%)	0.560 (-38%)	0.0167
$k_d = -80$, $c_d = 32$	0.512 (+1%)	0.570 (-18%)	0.561 (-38%)	0.0160
$k_d = -160$, $c_d = 28$	0.461 (-9%)	0.510 (-27%)	0.898 (-1%)	0.0155
$k_d = -200$, $c_d = 26$	0.429 (-15%)	0.486 (-30%)	0.976 (+8%)	0.0159
$k_d = -220$, $c_d = 24$	0.413 (-18%)	0.475 (-32%)	0.977 (+8%)	0.0160

As the absolute value of k_d increases, from Figure 3.8, the structural damping is increased, and the controller is becoming more aggressive. From Table 3.1, bigger structural damping results in smaller responses of maximum relative displacement and interstory drift, as we expected. However, the maximum acceleration is increased as $|k_d|$ increases. This is because the control forces are clipped by the force feedback loop.

Two VDNS control designs with different capabilities are selected to compare with the clipped-optimal controllers in [13]. VDNS A is designed by taking $k_d = -80$ N/cm, and $c_d = 32$ N-sec/cm. VDNS B is designed by taking $k_d = -220$ N/cm, and $c_d = 24$ N-sec/cm. The results show that VDNS A appears to be quite effective in achieving significant reductions in both the maximum absolute acceleration and interstory displacement over the passive case and clipped-optimal controller A. In the meanwhile, the maximum relative displacement of VDNS A is increased a little bit compared to the best passive case, which is much better than clipped-optimal controller A. VDNS B has the biggest reduction of interstory drift, which is 32% reduction as compared to the best passive case, and has comparable level of maximum relative displacement with clipped-optimal controller B, which is 18% reduction as compared to the best passive case. In the meanwhile, the increase of maximum acceleration (+8% compared to the best passive case) is much smaller than clipped-optimal controller B (+38%). The comparison of different control designs is given in Table 3.2.

Table 3.2: Evaluation Criteria of Different Control Designs.

Control Strategy	J_1	J_2	J_3	J_4
Passive-Off	0.862	0.801	0.904	0.00292
Passive-On	0.506	0.696	1.41	0.0178
Clipped-Optimal A	0.631 (+24%)	0.640 (-8%)	0.636 (-29%)	0.01095
Clipped-Optimal B	0.405 (-20%)	0.547 (-21%)	1.25 (+38%)	0.0178
VDNS A	0.512 (+1%)	0.570 (-18%)	0.561 (-38%)	0.016
VDNS B	0.413 (-18%)	0.475 (-32%)	0.977 (+8%)	0.016

Additionally, to compare the performance of the different control algorithms, the peak of the relative displacement, interstory drift and absolute acceleration responses for all floors were examined. Figure 3.9 shows the peak response profile of the entire structure for a variety of cases.

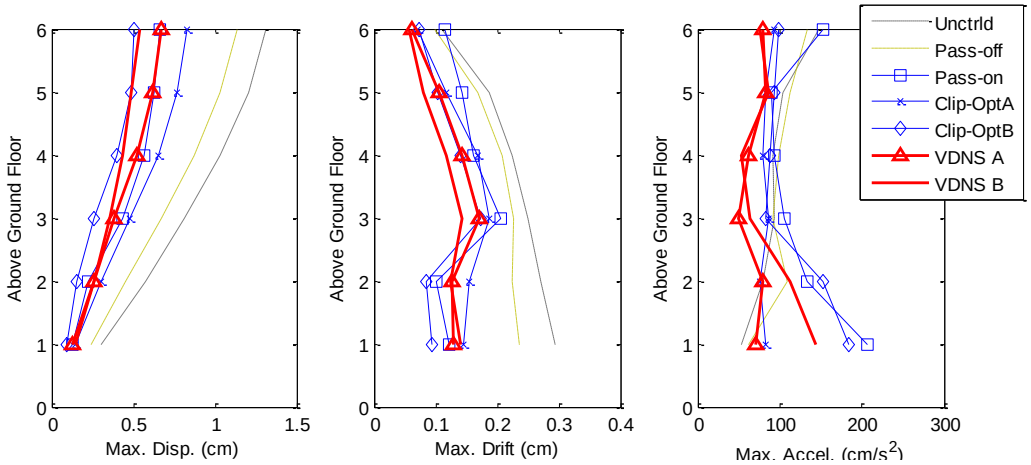

Figure 3.9: Peak Responses of Each Floor of the Building.

3.5. Summary

In this chapter, the viscous damping and negative stiffness (VDNS) control algorithm is provided for the response control of earthquake excited buildings. This algorithm is designed to increase the damping of structure to reduce the responses. It results in a very simple form of control force, which requires only the measurements of the relative displacement and relative velocity across the control device. Therefore, the control systems designed base on the VDNS algorithm can be implemented decentralized. In addition, the small amount of sensors and simple algorithm would reduce the source of errors and uncertainties.

A six-story building was used as an example to demonstrate the procedure of the design of VDNS controller. This building has been studied by Jansen et al.. The MR damper is

used as the control device, therefore a secondary controller or clipping algorithm is required to induce the MR damper to produce approximately the desired control force. Parametric study was conducted for the VDNS control system. It was observed that as the value of $|k_d|$ increases, the structural damping is increased, resulting in the reduction of the maximum relative displacement and interstory drift of the building, but the maximum absolute acceleration increases.

Two control systems were designed based on the VDNS algorithm, and the results are compared with the clipped optimal controllers provided in [13], and the passive cases as well. Both designed controllers are able to make the values of evaluation criteria $J_1 - J_3$ be less than one, indicating the controllers are effective to reduce the responses of the building, as compared to the uncontrolled case. The VDNS controller A achieves better results of the maximum interstory drift and the maximum absolute acceleration than the best passive case, and maintains the same level of peak relative displacement. In addition, it is found to be more effective than clipped optimal controller A. The VDNS controller B has better results of the maximum relative displacement and the maximum interstory drift than the best passive case, with slight increase in the maximum absolute acceleration. VDNS B is also found to be more effective than the clipped optimal controller B.

CHAPTER 4. CASE STUDY: 20-STORY LINEAR BENCHMARK BUILDING

In this chapter, the proposed VDNS control algorithm is applied to a model of a full scale building to verify its effectiveness. The model used in this study is the linear full scale 20-story building model developed for the benchmark control. The responses of the building, including the maximum and normed relative displacement, interstory drift ratio, acceleration, and required control forces, are evaluated due to various earthquake excitations. An active control system using 897 kN hydraulic actuators and a semi-active system employing 1000 kN MR dampers are developed based on the VDNS algorithm. The two control systems are evaluated for different models of the structure, corresponding to the structure before and after earthquake, to study the robustness of the algorithm.

4.1. Benchmark Building Description

The benchmark building used for case study herein is a full scale 20-story linear benchmark building. The building was designed by Brandow & Johnston Associates for the SAC Phase II Steel Project. It was designed to meet the seismic code and represents a typical mid- to high-rise building designed for the Los Angeles, California region, although it was not constructed. Detailed information about this 20-story linear building is provided in the benchmark problem statement [39].

This benchmark study focuses on an in-plane (2-D) analysis of one-half of the entire structure. The frame being considered is one of the N-S MRFs (the short, or weak, direction of the building). The height to width ratio for the N-S frame is 2.65:1. The N-S MRF is depicted in Figure 4.1. Control devices can be implemented throughout these N-S frames of the structure. The LA 20-story structure is modeled using 180 nodes

interconnected by 284 elements, as seen in Figure 4.2. The nodes are located at beam-to-column joints and at column splice locations. Elements are created between nodes to represent the beams and columns in the structure. Each element, modeled as a plane frame element, contains two nodes and six DOFs. The length, area, moment of inertia, modulus of elasticity and mass density are pre-defined for each element. The elemental consistent mass and stiffness matrices are determined as functions of these properties.

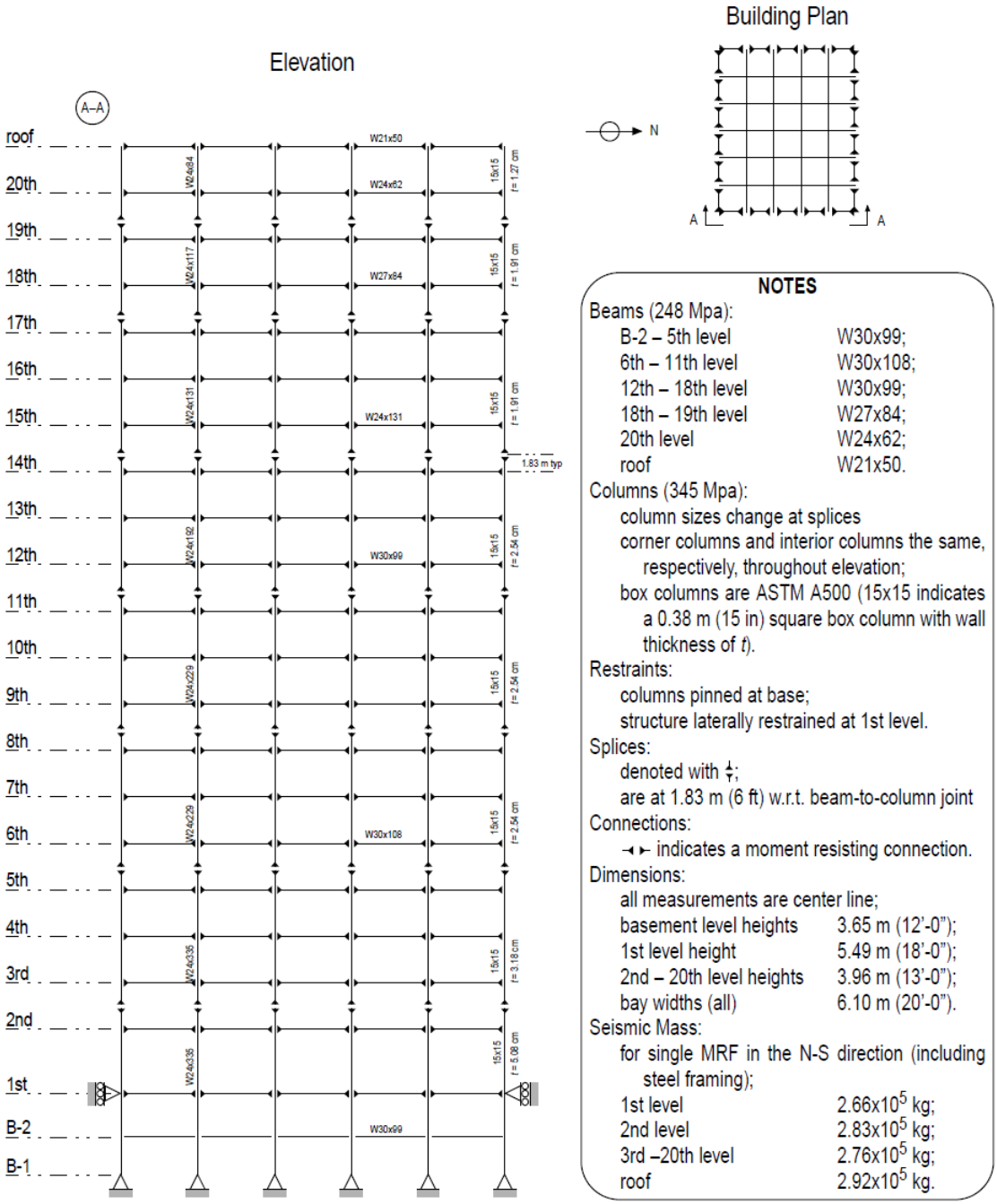

Figure 4.1: Los Angeles 20-Story Building N-S MRF [39].

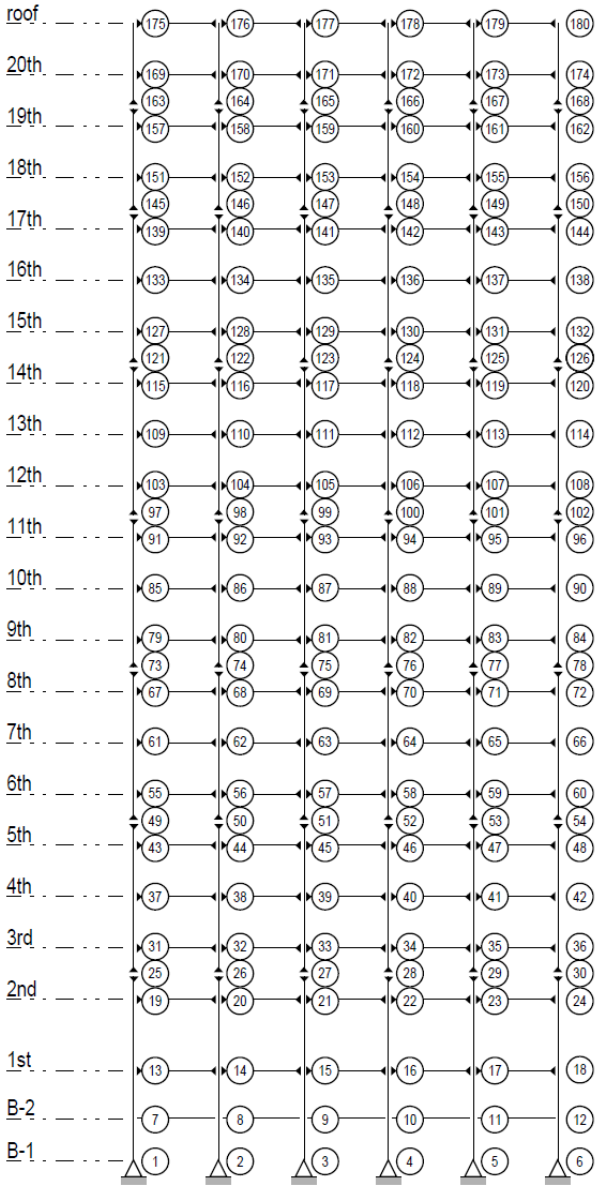

Figure 4.2: Node Numbers for the Los Angeles 20-Story Building N-S MRF [39].

4.2. Degradation Effects

The change of the dynamic properties of a building from before (pre-earthquake) to after (post-earthquake) a strong motion earthquake can be substantial. This change can cause as much as a 20% increase in the fundamental period, which is primarily due to stiffness

degradation. Such stiffness reduction is attributed to the loss of non-structural elements and to damage of structural elements. Because the time between the main earthquake and subsequent significant aftershocks may not be large, an effective control system should be sufficiently robust to perform adequately based either on the pre-earthquake structure or the post-earthquake structure.

Two evaluation models are developed: the pre-earthquake evaluation model and the post-earthquake evaluation model. These two models are intended to account for the degradation effects that can occur within the structure during a strong ground motion and should be viewed as liberalized models of the structure before and after degradation of the structure has occurred. The degradation of the benchmark building is modeled as a reduction in stiffness from the pre-earthquake to post-earthquake models. It should be noted that the post-earthquake building model assumes structural damage has occurred, which may be potentially avoided through the application of control devices. Therefore, the post-earthquake building model may be viewed in some sense as representing a "worst-case" scenario.

The pre-earthquake evaluation model represents the LA 20-story structure as-built. The as-built structure includes additional stiffness provided by the lateral resistance of the structure's gravity system and non-structural elements such as partitions and cladding. The non-structural elements are accounted for in the pre-earthquake evaluation model by proportionally increasing the structural stiffness matrix such that the first natural frequency of the evaluation model is 10% greater than that of the nominal model. The pre-earthquake damping is determined using this increased stiffness.

The post-earthquake evaluation model is intended to represent the LA 20-story structure after a strong motion earthquake. After a strong motion earthquake, the non-structural elements may no longer provide any additional stiffness to the structure. Moreover, the structural elements may be damaged, causing a decrease in stiffness. In this study, a post-earthquake evaluation model is developed in which the natural frequency of the structure

is decreased by 10% from the nominal structural model. This reduction is accomplished by an associated reduction in the structural stiffness matrix, corresponding to an 18.2% reduction in natural frequency from the pre-earthquake evaluation model to the post-earthquake evaluation model. The post-earthquake damping is determined using this decreased stiffness.

The first 10 natural frequencies of the pre-earthquake model are: 0.29, 0.83, 1.43, 2.01, 2.64, 3.08, 3.30, 3.53, 3.99 and 4.74 Hz. The first 10 natural frequencies of the post-earthquake model are: 0.24, 0.68, 1.17, 1.65, 2.16, 2.52, 2.70, 2.89, 3.26 and 3.88 Hz.

4.3. Control System Design

Two control systems have been developed based on the VDNS algorithm introduced in Chapter 3, and applied to the numerical models of the benchmark structure. Hydraulic actuators are used for the active control system to produce the control forces of VDNS algorithm. The control system employing MR dampers is also developed to investigate the application of VDNS algorithm in semi-active control. The phenomenological model of the MR damper and the modified clipping algorithm discussed in Chapter 2 is employed in the numerical simulation. Each control device is oriented horizontally, and is rigidly attached between the two adjacent floors of the building. The various components of the control systems (i.e., sensors, control devices) and design of VDNS control system are described in this section.

4.3.1. Sensors

The device displacements are measured using LVDTs. The the sensitivity of each LVDT is 100 V/m. The relative velocity of the control device is obtained by taking the difference of the absolute velocities between two floors where the device is attached. The absolute velocity measurements are approximated by passing the measured accelerations through a second order filter with the following transfer function [7]

$$H(s) = \frac{39.5s}{39.5s^2 + 8.98s + 1}. \tag{4.1}$$

The sensitivity of each accelerometer is 10 V/g. The semi-active control system also utilizes force feedback measurements from force transducers located on each device. The sensitivity of each force transducer is 10 V/1000 kN.

Control devices are implemented on all the twenty stories in this study. Therefore, the vector of measurements for control forces of the semi-active system is $\mathbf{f}_m = \left[f_{m1}, f_{m2}, \cdots, f_{m20} \right]^T$. One advantage of the VDNS algorithm is that it can be implemented decentralized. Only the measurements at the locations of the control devices are required. Thus, LVDTs and accelerometers are simulated on floors 1 to 20. In addition, another accelerometer is needed to measure the ground acceleration. So, the vector of measured responses is $\mathbf{y}_m = \left[\ddot{x}_g, \ddot{x}_{a1}, \ddot{x}_{a2}, \cdots, \ddot{x}_{a20}, x_{d1}, x_{d2}, \cdots, x_{d20} \right]^T$. As specified in the benchmark problem statement, each of these measured responses are assumed to contains an RMS noise of 0.03 Volts, which are modeled as Gaussian rectangular pulse processes with a pulse width of 0.01 sec.

4.3.2. Control Devices

Hydraulic actuators are chosen for the active control systems in this study. Typically in control design, device constraints are a major concern that needs to be addressed. These limitations could include device stroke, velocity, or force output. For the study, the active devices are considered to be ideal actuators with a maximum force output of 897 kN (200 kip) and a stroke of $\pm$8.9 cm ($\pm$3.5 in).

MR dampers are used for the semi-active control system in this study. The approach used for modeling of the MR damper was presented in Chapter 2. Yoshida [27] developed

parameters for the MR damper model to have a capacity of 1000 kN (224.8 kip) and are given as: α_a = 1.0872e5 N/cm, α_b = 4.96116e5 N/(cm-V), n = 1, A = 1.2, γ = 3 cm^{-1}, β = 3 cm^{-1}, η = 5 sec^{-1}, and $V_{\max}$ = 10 V. The scaled up MR damper is estimated to have a maximum power requirement of 50 Watts, according to the manufacturer. Device constraints such as stroke and velocity are neglected for the MR damper.

4.3.3. VDNS Controller

A state space representation of the input-output model for the LA 20-story structure was developed in the benchmark problem statement. The model is of the form

$$\dot{\mathbf{x}}_s = \mathbf{A}\mathbf{x}_s + \mathbf{B}\mathbf{f} + \mathbf{E}\ddot{x}_g \tag{4.2}$$

$$\mathbf{y}_m = \mathbf{C}_m\mathbf{x}_s + \mathbf{D}_m\mathbf{f} + \mathbf{F}_m\ddot{x}_g + \mathbf{v}_m \tag{4.3}$$

$$\mathbf{y}_e = \mathbf{C}_e\mathbf{x}_s + \mathbf{D}_e\mathbf{f} + \mathbf{F}_e\ddot{x}_g \tag{4.4}$$

$$\mathbf{z} = \mathbf{C}_z\mathbf{x}_s + \mathbf{D}_z\mathbf{f} \tag{4.5}$$

where $\mathbf{y}_m$ is the vector corresponding to measured outputs, $\mathbf{v}_m$ is a measurement noise vector, and $\mathbf{y}_e$ is the vector corresponding to the regulated outputs that are used for evaluation of the systems. $\mathbf{z} = \left[x_{N_1}, x_{N_2}, \cdots, x_{N_{20}}, \dot{x}_{N_1}, \dot{x}_{N_2}, \cdots, \dot{x}_{N_{20}} \right]^T$ is a vector which represents the set of states corresponding to the horizontal displacements and velocities of all floors relative to the ground.

All 20 floors are implemented with control devices in the design of control system. The desired control force of the *i*th control device according to the VDNS algorithm is given as

$$f_{di} = k_{di} d_i + c_{di} v_i \tag{4.6}$$

where d_i and v_i are the relative displacement and velocity across the ith control device, k_{di} is the negative stiffness coefficient, which has to be negative, and c_{di} is the damping coefficient, which has to be positive. Let all desired control forces have the same value of k_d and c_d, therefore, the vector of control force **f** can be written as

$$\mathbf{f} = \begin{Bmatrix} f_1 \\ f_2 \\ \vdots \\ f_n \end{Bmatrix} = \begin{Bmatrix} k_d x_{N_1} + c_d \dot{x}_{N_1} \\ k_d (x_{N_2} - x_{N_1}) + c_d (\dot{x}_{N_2} - \dot{x}_{N_1}) \\ \vdots \\ k_d (x_{N_n} - x_{N_{n-1}}) + c_d (\dot{x}_{N_n} - \dot{x}_{N_{n-1}}) \end{Bmatrix} = \mathbf{Tz} \tag{4.7}$$

where $\mathbf{T} = \begin{bmatrix} \mathbf{K}_d & \mathbf{C}_d \end{bmatrix}$ consists of the negative stiffness matrix $\mathbf{K}_d$ and the control damping matrix $\mathbf{C}_d$, and

$$\mathbf{K}_d = \begin{bmatrix} k_d & 0 & \cdots & 0 & 0 \\ -k_d & k_d & & 0 & 0 \\ \vdots & & \ddots & \vdots & \\ 0 & 0 & & k_d & 0 \\ 0 & 0 & \cdots & -k_d & k_d \end{bmatrix} \tag{4.8}$$

$$\mathbf{C}_d = \begin{bmatrix} c_d & 0 & \cdots & 0 & 0 \\ -c_d & c_d & & 0 & 0 \\ \vdots & & \ddots & \vdots & \\ 0 & 0 & & c_d & 0 \\ 0 & 0 & \cdots & -c_d & c_d \end{bmatrix}. \tag{4.9}$$

Using Eq. (4.5) in Eq. (4.7),

$$\mathbf{f} = \mathbf{Tz} = \mathbf{T}\left(\mathbf{C}_z\mathbf{x}_s + \mathbf{D}_s\mathbf{f}\right). \tag{4.10}$$

Therefore,

$$\mathbf{f} = \left(\mathbf{I} - \mathbf{TD}_z\right)^{-1}\mathbf{TC}_z\mathbf{x}_s. \tag{4.11}$$

Using Eq. (4.11) in Eq. (4.2), the controlled system becomes

$$\dot{\mathbf{x}}_s = \mathbf{A}_c\mathbf{x}_s + \mathbf{E}_c\ddot{x}_g \tag{4.12}$$

where

$$\mathbf{A}_c = \mathbf{A} + \mathbf{B}\left(\mathbf{I} - \mathbf{TD}_z\right)^{-1}\mathbf{TC}_z. \tag{4.13}$$

In most cases, $\mathbf{D}_z = \mathbf{0}$. The poles $\lambda_m = -\sigma_m \pm i\omega_{d,m}$ of the controlled system can be determined by calculating the eigenvalues of the state matrix $\mathbf{A}_c$. To ensure that the controlled system is stable, all eigenvalues of $\mathbf{A}_c$ must have negative real parts, i.e., $\sigma_m > 0$. The damping ratio of the first mode of the controlled structure ζ_1 can be calculated as

$$\zeta_1 = \frac{\sigma_1}{\omega_{n,1}} = \frac{\sigma_1}{\sqrt{\sigma_1^2 + \omega_{d,1}^2}}. \tag{4.14}$$

Because the evaluation model is quite large, a reduced order model of the system is developed for purposes of control design in the benchmark problem definition, and the reduced model is employed in this study as well. k_d and c_d are chosen as –10000 kN/m and 40000 kN-sec/m respectively. Figure 4.3(a) and (b) show the poles of the control

system of the reduced order model, all of which are located in the left half plane (LHP). Because the reduced model is based on the pre-earthquake model of the structure, it is observed to have the same poles as those kept in the full pre-earthquake model, as shown in Figure 4.3(c) and (d). Figure 4.3(e) and (f) give the locations of poles for the post-earthquake model, and all of the poles are also located in LHP. Therefore, the control system developed based on VDNS algorithm is stable for both pre-earthquake and post-earthquake structures.

Northridge earthquake was used to determine the number of control devices on each floor because it requires the largest control forces in the structure. In the active control system, the numbers of hydraulic actuators located at floors from 1 to 20 are [10, 8, 7, 7, 6, 6, 6, 5, 5, 5, 4, 4, 4, 4, 4, 3, 3, 3, 2, 2]. The total number of control devices is 98. In the semi-active control system, the numbers of MR dampers located at floors from 1 to 20 are [9, 7, 6, 6, 5, 5, 5, 5, 4, 4, 4, 4, 3, 3, 4, 3, 3, 2, 2, 2]. The total number of devices is 86. The Simulink model of the simulation is shown in Figure 4.4. The Dormand–Prince method is employed as the integrator and the integration step is 0.0005 sec.

4.4. Evaluation Criteria

The controllers are evaluated under four earthquake records provided in the benchmark problem statement [39]: (i) El Centro; (ii) Hachinohe; (iii) Northridge; (iv) Kobe. The power spectra of the earthquakes are shown in Figure 4.5. To evaluate the control algorithm, the first fourteen evaluation criteria defined in the benchmark problem statement are evaluated for each control design. All of evaluation criteria are summarized in Table 4.1 [39]. For the semi-active system, the evaluation criteria describing the required maximum control power J_{13} and normed control power J_{14}, are calculated by assuming that the maximum power is required for each MR damper when it is ON.

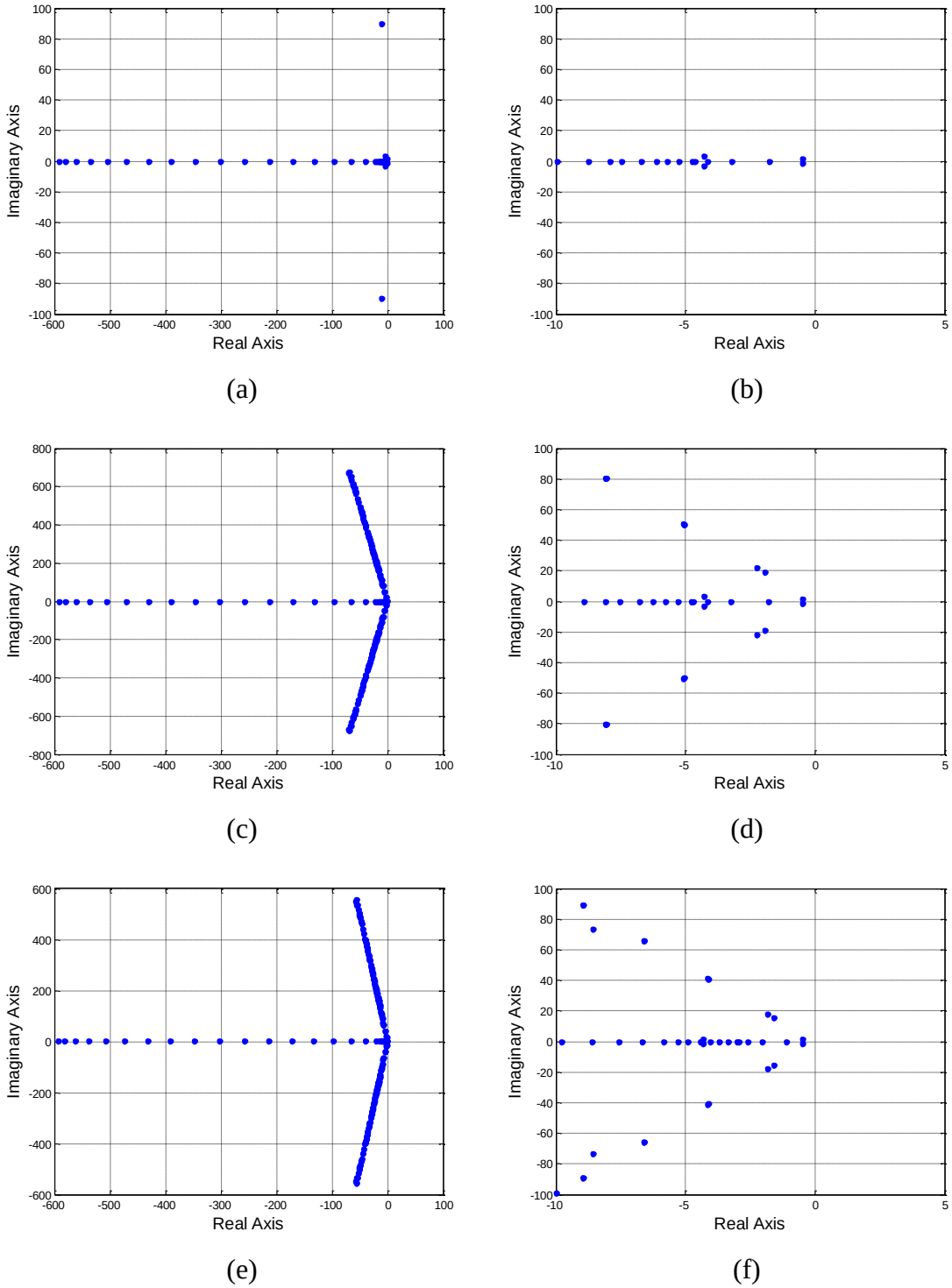

Figure 4.3: Poles Locations of the Controlled Structure.

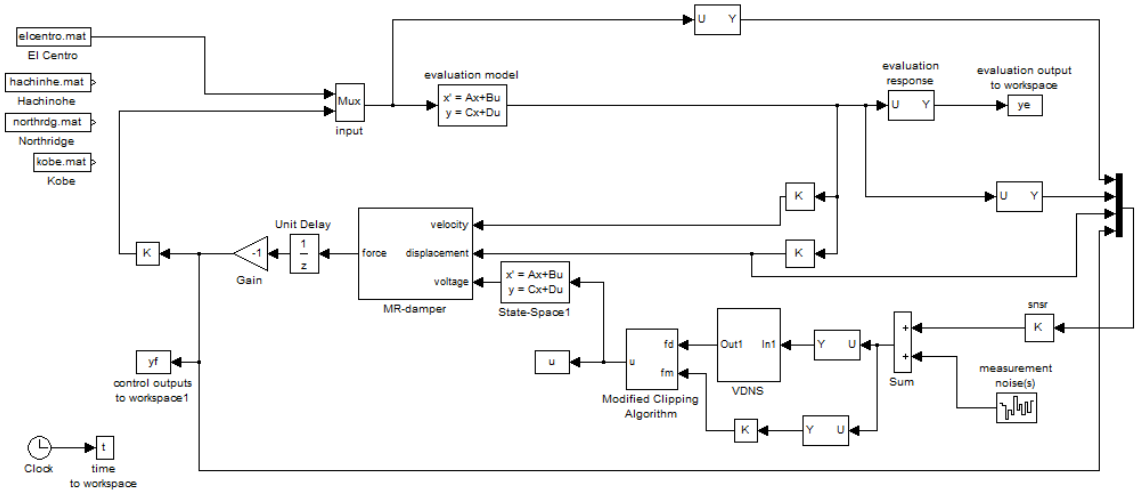

Figure 4.4: Simulink Model for Control System.

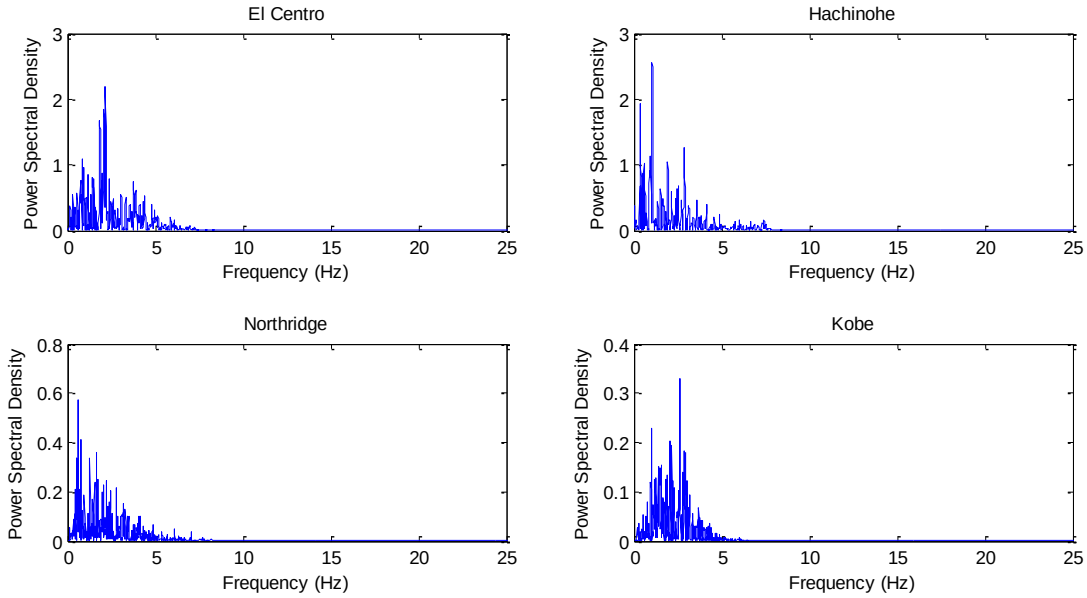

Figure 4.5: Power Spectra of Earthquakes.

Table 4.1: Summary of Evaluation Criteria [39].

Floor Displacement $J_1 = \max_{\text{El Centro, Hachinohe, Northridge, Kobe}} \left\{ \frac{\max_{t,\, l \in \eta} \lvert x_l(t) \rvert}{x^{\max}} \right\}$	Normed Floor Displacement $J_5 = \max_{\text{El Centro, Hachinohe, Northridge, Kobe}} \left\{ \frac{\max_{l \in \eta} \lVert x_l(t) \rVert}{\lVert x^{\max} \rVert} \right\}$	Control Force $J_9 = \max_{\text{El Centro, Hachinohe, Northridge, Kobe}} \left\{ \frac{\max_{t,\, l} \lvert f^d(t) \rvert}{W} \right\}$	Control Devices J_{13} = number of control devices required
Interstory Drift $J_2 = \max_{\text{El Centro, Hachinohe, Northridge, Kobe}} \left\{ \frac{\max_{t,\, l} \left(\frac{\lvert d_l(t) \rvert}{h_l} \right)}{d_n^{\max}} \right\}$	Normed Interstory Drift $J_6 = \max_{\text{El Centro, Hachinohe, Northridge, Kobe}} \left\{ \frac{\max_{t,\, l} \left(\frac{\lVert d_l(t) \rVert}{h_l} \right)}{\lVert d_n^{\max} \rVert} \right\}$	Control Device Stroke $J_{10} = \max_{\text{El Centro, Hachinohe, Northridge, Kobe}} \left\{ \frac{\max_{t,\, l} \lvert y_l^a(t) \rvert}{x^{\max}} \right\}$	Sensors J_{14} = number of sensors required
Floor Acceleration $J_3 = \max_{\text{El Centro, Hachinohe, Northridge, Kobe}} \left\{ \frac{\max_{t,\, l \in \eta} \lvert \ddot{x}_{al}(t) \rvert}{\ddot{x}_a^{\max}} \right\}$	Normed Floor Acceleration $J_7 = \max_{\text{El Centro, Hachinohe, Northridge, Kobe}} \left\{ \frac{\max_{l \in \eta} \lVert \ddot{x}_{al}(t) \rVert}{\lVert \ddot{x}_a^{\max} \rVert} \right\}$	Control Power $J_{11} = \max_{\text{El Centro, Hachinohe, Northridge, Kobe}} \left\{ \frac{\max_{t} \left[\sum_l \mathcal{P}_l(t) \right]}{\dot{x}^{\max} W} \right\}$	
Base Shear $J_4 = \max_{\text{El Centro, Hachinohe, Northridge, Kobe}} \left\{ \frac{\max_{t} \left\lvert \sum_{l=1}^{20} m_l \ddot{x}_{a\eta_l}(t) \right\rvert}{F_b^{\max}} \right\}$	Normed Base Shear $J_8 = \max_{\text{El Centro, Hachinohe, Northridge, Kobe}} \left\{ \frac{\left\lVert \sum_{l=1}^{20} m_l \ddot{x}_{a\eta_l}(t) \right\rVert}{\lVert F_b^{\max} \rVert} \right\}$	Normed Control Power $J_{12} = \max_{\text{El Centro, Hachinohe, Northridge, Kobe}} \left\{ \frac{\sum_l \lVert \mathcal{P}_l(t) \rVert}{\dot{x}^{\max} W} \right\}$	

4.5. Numerical Results

4.5.1. Active Control System

The performance of the active control system of VDNS algorithm using hydraulic actuators is first assessed. The control design is evaluated for all four earthquake records, and for both the pre-earthquake and post-earthquake evaluation models described previously as well.

The resulting evaluation criteria for this control design are presented in Table 4.2 (pre-earthquake) and Table 4.3 (post-earthquake). In these tables, the evaluation criteria are shown for each earthquake, and the maximum value over all four earthquakes is provided

in the last column. Additionally, the maximum values of the control constraints are provided for each earthquake.

Note that for the pre-earthquake study, the designed active control system based on the VDNS algorithm is able to reduce the normed responses of the building significantly under all four earthquake excitations. This is indicated by the evaluation criteria $J_5 - J_8$, whose values are all far less than one. The values of the peak responses $J_1 - J_4$ are also less than one for the active control system, except that the peak base shear under Northridge earthquake is slightly greater than the uncontrolled case, indicating that the control system is also effective to reduce the peak responses. From Table 4.2, the control system reduces the maximum relative displacement by 50.1–67.0%, the maximum normalized drift by 35.9–62.1%, and the maximum absolute acceleration by 7.3–32.8% as compared to the uncontrolled values. Figure 4.6 shows a series of plots portraying certain maximum responses of the building. For each earthquake, the maximum value of the non-dimensionalized interstory drift at each floor above ground, and the maximum value of the absolute acceleration at each floor above ground, are plotted. It is observed that the peak interstory drifts and the peak absolute accelerations are reduced at all floors for all earthquake excitations, as compared to the uncontrolled cases. Figure 4.6 also shows the responses of the roof of the building over time for each earthquake. For clarity, only the first 80 seconds of the responses are shown. In these plots one observes that the control system not only reduces the peak response, but is also able to relatively quickly dampen out the responses of the building.

Although the control system is designed based on the pre-earthquake model of the building, the control strategy maintains its effectiveness in the post-earthquake structure as well. The normed responses of the post-earthquake structure are substantially reduced, as demonstrated quantitatively by the values of the evaluation criteria $J_5 - J_8$ as shown in Table 4.3. The maximum relative displacements and maximum non-dimensionalized interstory drifts of the structure are reduced by 35.3–57.1% and 25.2–62.8% of the uncontrolled values, respectively. Figure 4.7 shows the time histories of the displacement

of the roof relative to the ground for all earthquakes. However, the reductions of the maximum floor accelerations and the maximum base shear are not as effective for the post-earthquake structure as for the pre-earthquake model. The reason might be the relative lower stiffness of the post-earthquake structure after strong earthquake motion. When the same control force is applied by the control algorithm, the whole structure becomes relatively stiffer for the post-earthquake model, which might cause high acceleration at certain floors where the control devices are attached. In Figure 4.7, the maximum value of the non-dimensionalized interstory drift at each floor above ground, and the maximum value of the absolute acceleration at each floor above ground are plotted. It is shown that the maximum interstory drifts are reduced substantially at all floors for every earthquake. Reductions of the maximum absolute accelerations at all floors are also observed for all earthquakes, except the 1st floor under El Centro earthquake.

4.5.2. Semi-Active Control System

To study the effectiveness of the application of the VDNS algorithm in the semi-active control, MR dampers are employed as the semi-active control devices to produce the control forces to the benchmark building. The VDNS controller designed in Section 4.3.3 is used as the nominal controller for the semi-active system. The control input to the MR damper is determined by the modified clipping algorithm discussed in Section 2.3 to generate the control force.

The performance of the semi-active control system in reducing the responses of the building is similar to that of the active system for different earthquakes. The normed responses ($J_5 - J_8$) are reduced substantially for both pre-earthquake and post-earthquake structures. For the pre-earthquake model, the values of the peak responses $J_1 - J_4$ are also less than one for most cases, except that the peak base shear under Northridge earthquake is slightly greater than the uncontrolled case. For the post-

earthquake model, the maximum relative displacements J_1 and maximum non-dimensionalized interstory drift J_2 are reduced as compared to the uncontrolled case, but the reduction of the maximum floor accelerations J_3 and the maximum base shear J_4 is not as effective.

One can compare the performances of active and semi-active systems visually in Figure 4.6 and Figure 4.7. It is found that the semi-active control system has comparable reduction of the relative displacements of the building to the active system. The peak interstory drifts at floors above ground of two control systems have similar profiles, while the peak absolute acceleration of the semi-active control system is generally greater than the active system at each floor. The acceleration levels of the semi-active system at upper floors are typically reduced significantly as compared to the uncontrolled case, although some increases in the acceleration levels are observed at the lower floors, because more control devices are attached at the lower floors. The big interstory drift of the building under Northbridge and Kobe earthquakes would cause the building to yield. And the nonlinear behavior due to the yielding are reduced and even eliminated by the control systems, as the drift ratios are reduced significantly.

The results of both the active control system and the semi-active system are compared with the results of a sample control system for both pre-earthquake structure (Figure 4.8) and post-earthquake structure (Figure 4.9). The sample controller is based on the LQG method and is explained in detail in the benchmark problem statement. The results of the sample control system are provided again in Table 4.6 and Table 4.7 for comparison. It is observed again that the active and semi-active control systems have comparable performance in reducing the peak relative displacement and the peak interstory drift, and both of them are more effective than the sample controller. Better results are observed for the semi-active system in the normed interstory drift comparing to the active system and the sample control system. The active system and the sample controller have close performance in the reduction of acceleration of the building, while the semi-active system is less effective to reduce the acceleration.

The magnitudes of the ratios of power spectral density functions for the semi-active control system are compared to those of the uncontrolled system in Figure 4.10. In this figure, the ratios from the ground acceleration to the displacement, velocity and acceleration at the first floor of the pre-earthquake building are plotted under El Centro earthquake. Notice that the peaks of the ratios of the controlled building are smaller than those of the uncontrolled transfer functions. It is observed that the magnitude of the controlled building from ground to the first floor acceleration is slightly increased at higher frequencies. The reason might be that the accelerations of the building is more affected by the higher modes than the displacements and velocities, and only the first mode was considered during the design of the control system. This also coincides with the observation that the designed control system is more effective to reduce the displacements and velocities of the building than the accelerations.

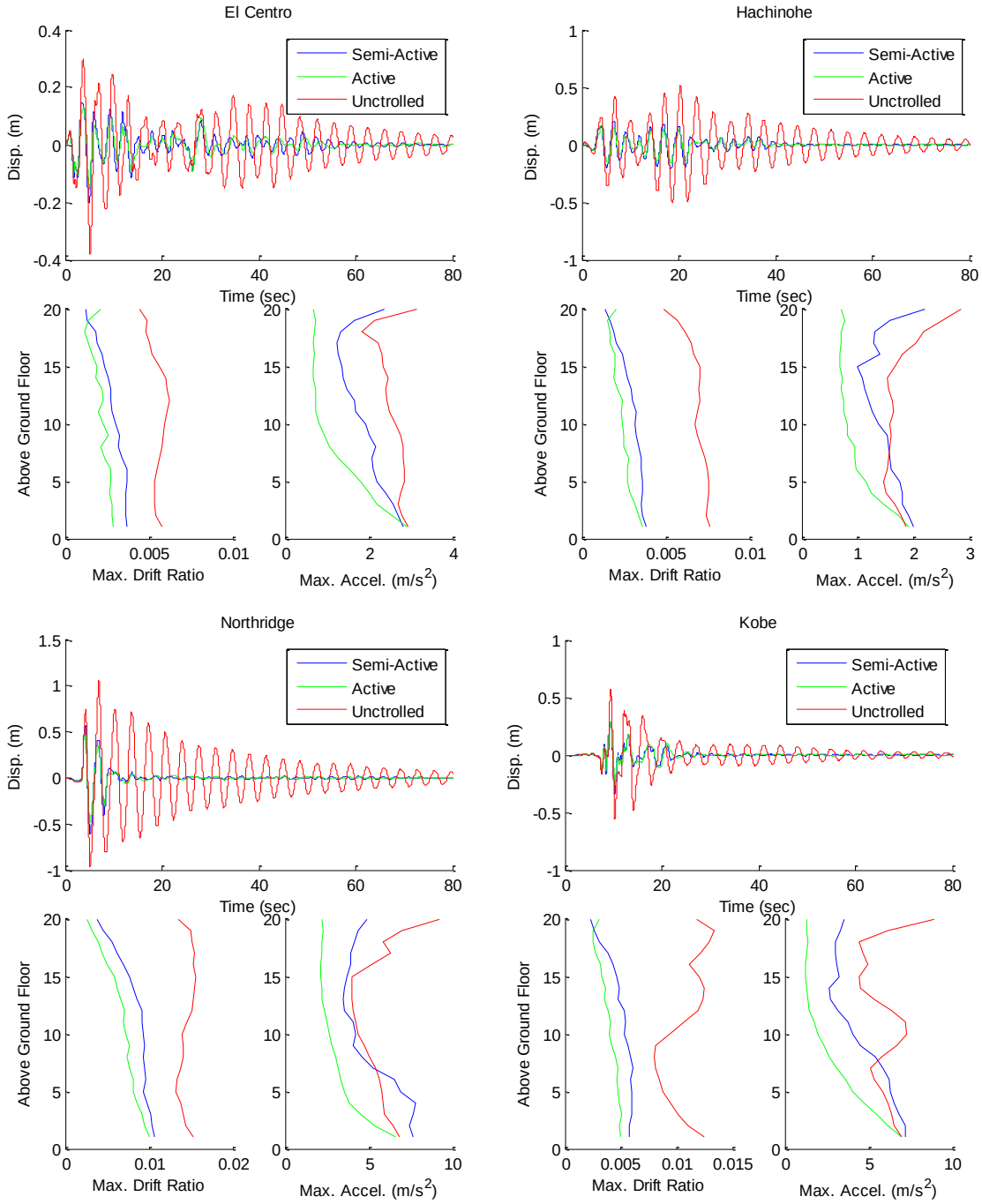

Figure 4.6: Comparison of Controlled and Uncontrolled Responses (Pre-Earthquake).

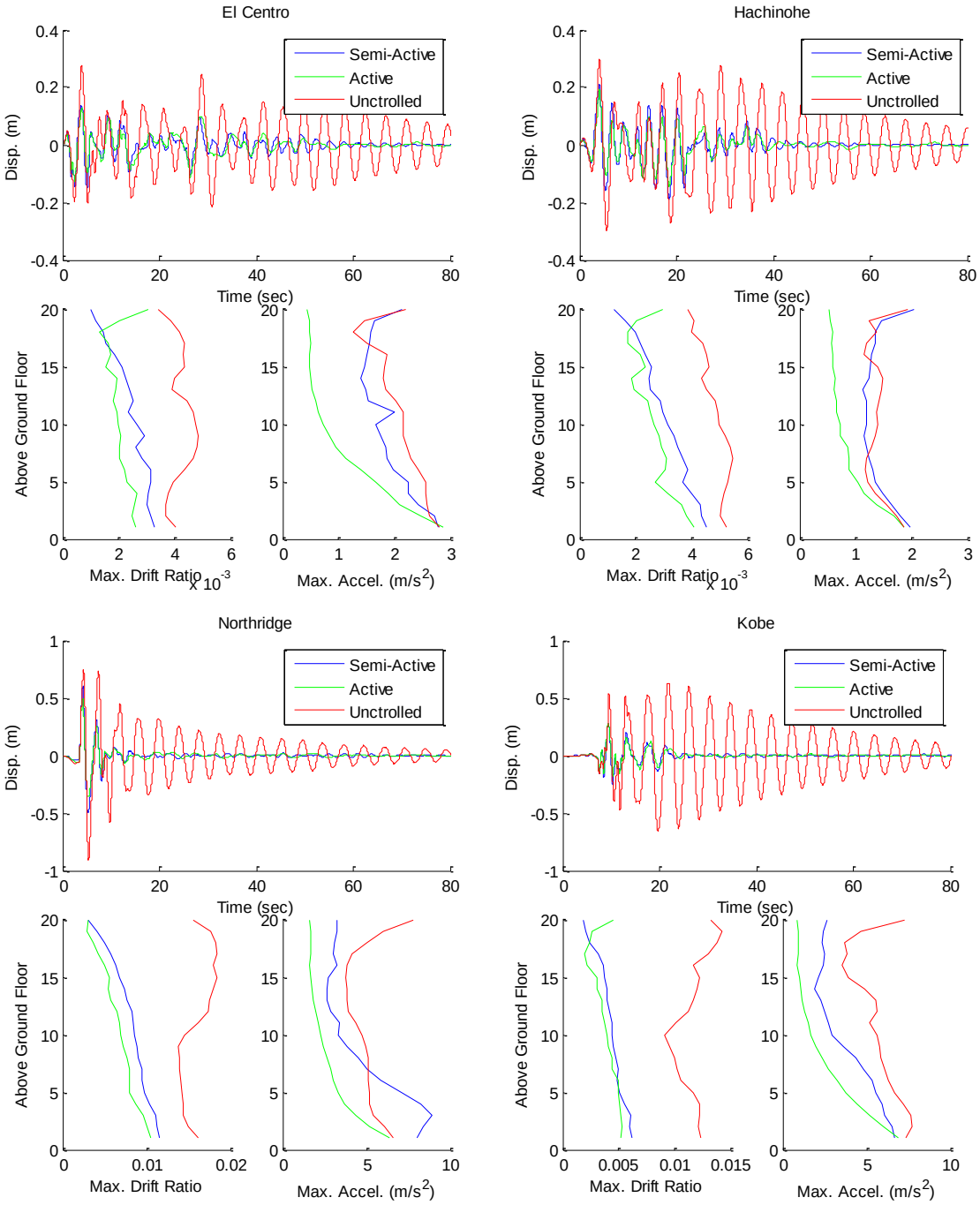

Figure 4.7: Comparison of Controlled and Uncontrolled Responses (Post-Earthquake).

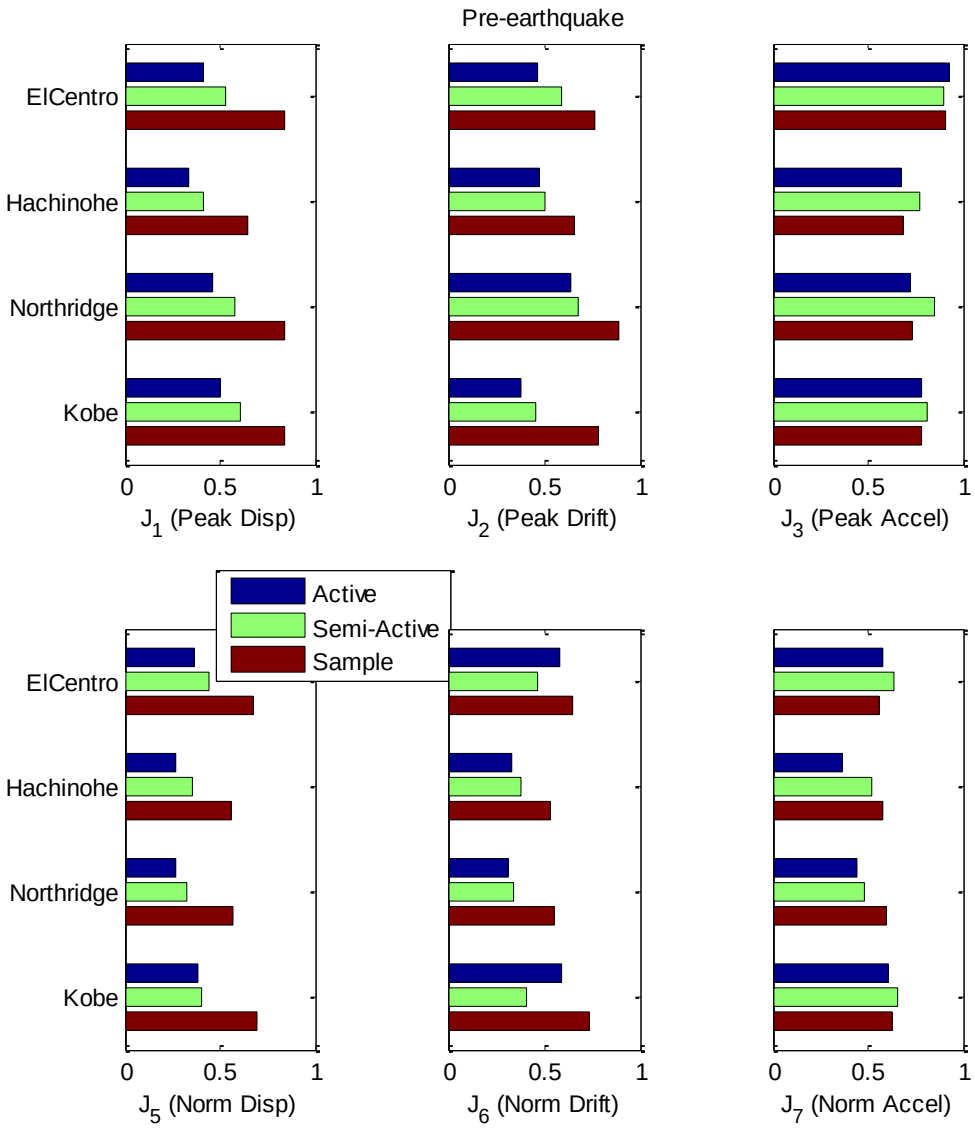

Figure 4.8: Bar Chart Comparing the Evaluation Criteria for Pre-Earthquake Model.

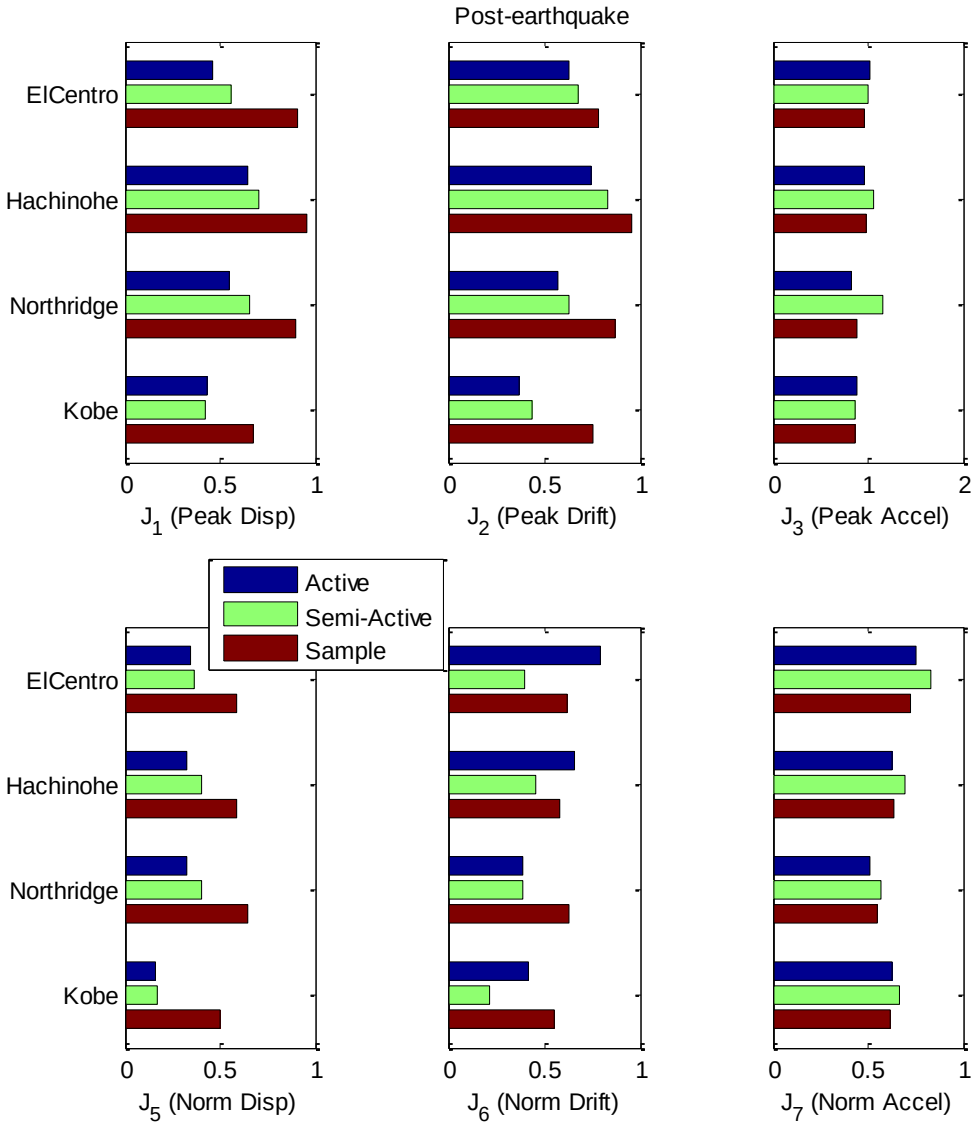

Figure 4.9: Bar Chart Comparing the Evaluation Criteria for Post-Earthquake Model.

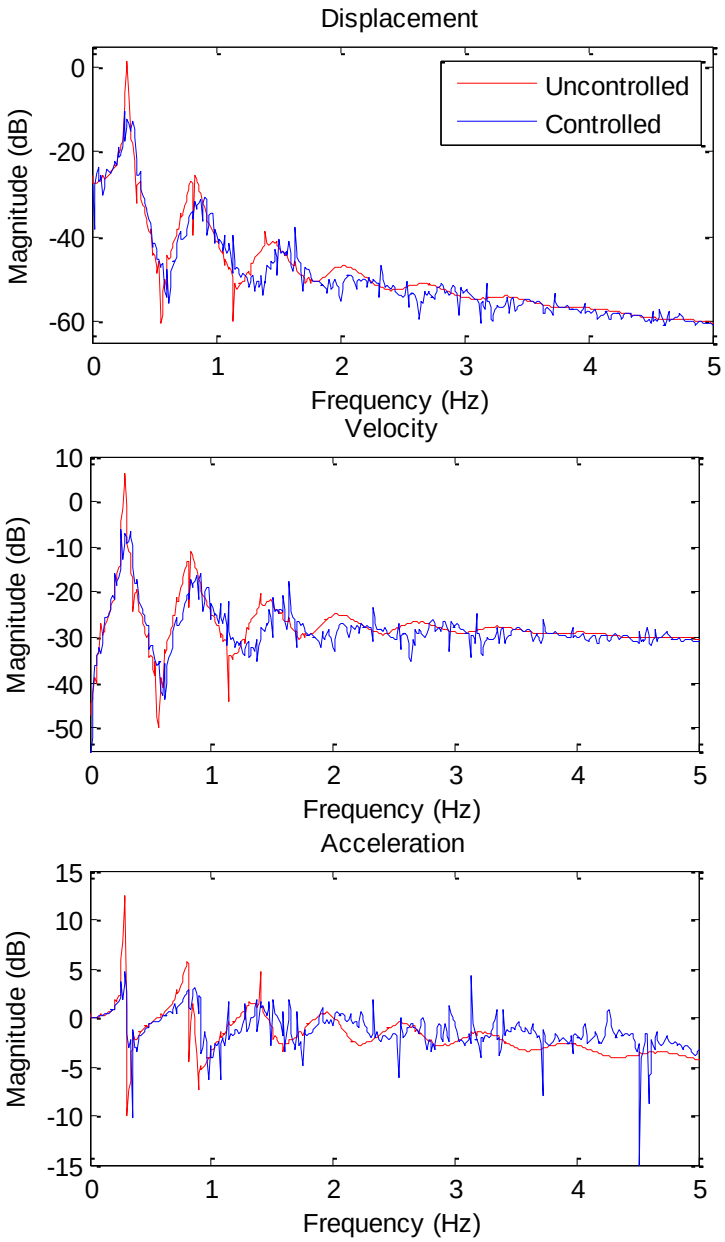

Figure 4.10: Ratios of Power Spectral Density Functions from Ground Acceleration to the First Floor Responses.

Table 4.2: Pre-Earthquake Evaluation Criteria for Active Control System.

	El Centro	Hachinohe	Northridge	Kobe	Max Value
J_1	0.409593	0.330556	0.461942	0.498787	0.498787
J_2	0.461923	0.476295	0.640581	0.379381	0.640581
J_3	0.926808	0.672309	0.722794	0.77899	0.926808
J_4	0.96136	0.657561	1.0904	0.847676	1.0904
J_5	0.363671	0.268029	0.266699	0.387001	0.387001
J_6	0.584397	0.329529	0.31432	0.594257	0.594257
J_7	0.576808	0.361838	0.445285	0.610601	0.610601
J_8	0.524599	0.350499	0.375204	0.673255	0.673255
J_9	0.00932626	0.00932537	0.0164856	0.0160326	0.0164856
J_{10}	0.0416193	0.0385525	0.0519467	0.0484308	0.0519467
J_{11}	0.01824	0.0117523	0.0425261	0.0476608	0.0476608
J_{12}	0.0359887	0.0271075	0.0926864	0.119329	0.119329
J_{13}	98				
J_{14}	41				
$\max_{i,t}\lvert u_i \rvert$ (V)	4.26156	4.26115	7.5094	7.29797	7.5094
$\max_{i,t}\lvert y_i^a \rvert$ (m)	0.0157983	0.0199336	0.0550167	0.0275508	0.0550167
$\max_{i,t}\lvert f^i \rvert$ (kN)	507.134	507.085	896.436	871.806	896.436

Table 4.3: Post-Earthquake Evaluation Criteria for Active Control System.

	El Centro	Hachinohe	Northridge	Kobe	Max Value
J_1	0.465108	0.646939	0.547181	0.429078	0.646939
J_2	0.634438	0.747491	0.569795	0.371943	0.747491
J_3	1.02291	0.957104	0.823839	0.887274	1.02291
J_4	1.89749	1.19804	1.34362	1.23558	1.89749
J_5	0.340113	0.321475	0.328939	0.162932	0.340113
J_6	0.794106	0.654323	0.391571	0.420428	0.794106
J_7	0.752423	0.62454	0.514141	0.621811	0.752423
J_8	0.602536	0.538537	0.566679	0.441936	0.602536
J_9	0.00918375	0.0091826	0.015767	0.0162577	0.0162577
J_{10}	0.0520016	0.0752031	0.0637042	0.0438298	0.0752031
J_{11}	0.0169939	0.0131137	0.0395741	0.0524428	0.0524428
J_{12}	0.0425576	0.036951	0.0930665	0.0967495	0.0967495
J_{13}	98				
J_{14}	41				
$\max_{i,t}\lvert u_i \rvert$ (V)	4.21016	4.20963	7.19547	7.40661	7.40661
$\max_{i,t}\lvert y_i^a \rvert$ (m)	0.0144497	0.0224339	0.0578212	0.0287598	0.0578212
$\max_{i,t}\lvert f^i \rvert$ (kN)	499.385	499.322	857.36	884.043	884.043

Table 4.4: Pre-Earthquake Evaluation Criteria for Semi-Active Control System.

	El Centro	Hachinohe	Northridge	Kobe	Max Value
J_1	0.531113	0.412962	0.581453	0.603492	0.603492
J_2	0.59043	0.504654	0.681825	0.45346	0.681825
J_3	0.895403	0.773268	0.851686	0.805963	0.895403
J_4	0.929798	0.680892	1.09529	0.836865	1.09529
J_5	0.442744	0.356359	0.326035	0.402454	0.442744
J_6	0.46913	0.382851	0.337438	0.409614	0.46913
J_7	0.63703	0.516389	0.478426	0.654141	0.654141
J_8	0.671658	0.497874	0.422268	0.677896	0.677896
J_9	0.008118	0.00782025	0.0170844	0.014869	0.0170844
J_{10}	0.0530512	0.040848	0.0552912	0.0551352	0.0552912
J_{11}	0.0000304	0.0000193	0.0000198	0.0000262	0.0000304
J_{12}	0.0001564	0.0001193	0.0000835	0.0001670	0.0001670
J_{13}	86				
J_{14}	61				
$\max_{i,t}\lvert u_i \rvert$ (V)	10	10	10	10	10
$\max_{i,t}\lvert y_i^a \rvert$ (m)	0.0201377	0.0211205	0.0585589	0.0313648	0.0585589
$\max_{i,t}\lvert f^i \rvert$ (kN)	441.433	425.242	929.001	808.533	929.001

Table 4.5: Post-Earthquake Evaluation Criteria for Semi-Active System.

	El Centro	Hachinohe	Northridge	Kobe	Max Value
J_1	0.561381	0.700934	0.659729	0.418342	0.700934
J_2	0.67359	0.830512	0.625755	0.433519	0.830512
J_3	0.990519	1.04941	1.14612	0.858309	1.14612
J_4	1.78191	1.25884	1.32837	1.16985	1.78191
J_5	0.359871	0.404711	0.404784	0.173486	0.404784
J_6	0.397573	0.452483	0.386805	0.21705	0.452483
J_7	0.826559	0.694292	0.565025	0.669214	0.826559
J_8	0.677791	0.680434	0.57377	0.432115	0.680434
J_9	0.0069155	0.00674475	0.0162669	0.0134758	0.0162669
J_{10}	0.0647521	0.0835556	0.0699607	0.0515888	0.0835556
J_{11}	0.0000274	0.0000264	0.0000184	0.0000283	0.0000283
J_{12}	0.0002074	0.0001934	0.0000898	0.0001413	0.0002074
J_{13}	86				
J_{14}	61				
$\max_{i,t}\lvert u_i \rvert$ (V)	10	10	10	10	10
$\max_{i,t}\lvert y_i^a \rvert$ (m)	0.0179927	0.0249255	0.0634998	0.033851	0.0634998
$\max_{i,t}\lvert f^i \rvert$ (kN)	376.044	366.759	884.544	732.775	884.544

Table 4.6: Pre-Earthquake Evaluation Criteria for Sample Control System.

	El Centro	Hachinohe	Northridge	Kobe	Max Value
J_1	0.83641	0.64297	0.84169	0.83707	0.84169
J_2	0.76526	0.66295	0.89064	0.77989	0.89064
J_3	0.90873	0.68122	0.73076	0.77925	0.90873
J_4	0.82445	0.68637	0.92953	0.75013	0.92953
J_5	0.67900	0.55644	0.56908	0.69826	0.69826
J_6	0.64982	0.53422	0.54936	0.73189	0.73189
J_7	0.56290	0.57347	0.59964	0.62149	0.62149
J_8	0.65736	0.53545	0.54906	0.70146	0.70146
J_9	0.0051430	0.0044520	0.011703	0.013881	0.013881
J_{10}	0.063221	0.053661	0.072224	0.10050	0.10050
J_{11}	0.0060031	0.0039088	0.013172	0.019699	0.019699
J_{12}	0.017602	0.016059	0.046692	0.066554	0.066554
J_{13}	50				
J_{14}	5				
$\max_{i,t}\lvert u_i \rvert$ (V)	2.3322	2.0185	5.3437	6.3193	6.3193
$\max_{i,t}\lvert y_i^a \rvert$ (m)	0.023998	0.027745	0.076493	0.057171	0.076493
$\max_{i,t}\lvert f^i \rvert$ (kN)	279.66	242.08	636.37	754.79	754.79

Table 4.7: Post-Earthquake Evaluation Criteria for Sample Control System.

	El Centro	Hachinohe	Northridge	Kobe	Max Value
J_1	0.90540	0.95701	0.89536	0.67871	0.95701
J_2	0.78630	0.95220	0.87461	0.75342	0.95220
J_3	0.96364	0.98872	0.87791	0.86729	0.98872
J_4	1.0237	1.0098	1.0226	0.83770	1.0237
J_5	0.58421	0.58789	0.64182	0.49803	0.64182
J_6	0.61935	0.58410	0.62597	0.55642	0.62597
J_7	0.72267	0.63379	0.54427	0.61833	0.72267
J_8	0.58675	0.54101	0.57136	0.52146	0.58675
J_9	0.0047313	0.0040596	0.010589	0.012992	0.012992
J_{10}	0.075587	0.095798	0.097784	0.089657	0.097784
J_{11}	0.0043104	0.0028936	0.012276	0.014300	0.014300
J_{12}	0.016151	0.013715	0.043397	0.049986	0.049986
J_{13}	50				
J_{14}	5				
$\max_{i,t}\lvert u_i \rvert$ (V)	2.0915	1.8060	4.7344	5.7984	5.7984
$\max_{i,t}\lvert y_i^a \rvert$ (m)	0.021003	0.028578	0.088753	0.058830	0.088753
$\max_{i,t}\lvert f^i \rvert$ (kN)	257.28	220.75	575.81	706.44	706.44

4.6. Summary

This chapter focuses on the application of the proposed VDNS control to a linear full scale building to verify the effectiveness of the control strategy. The full scale building used in this chapter is the 20-story building used for the benchmark study. To investigate the achievable capabilities of the control algorithm, two control systems were developed and evaluated, including an active control system using 897 kN hydraulic actuators, and a

semi-active system using 1000 kN MR dampers. Control devices are implemented on all 20 floors above ground of the building. Both control systems are designed to be decentralized because of the specialty of the VDNS algorithm. Only the relative displacement and relative velocity across the control device are needed for the controller of each control device. The device displacement is measured directly, and the device velocity is derived from the absolute accelerations measured at the adjacent floors. In addition, the semi-active control system also employed measurements of the forces produced by each device for control force determination. The MR damper was controlled using the modified clipping algorithm to produce the desired control force.

Both of the designed active and semi-active control systems are able to substantially reduce the normed responses of the building. The maximum relative displacement and the maximum interstory drift responses are reduced significantly. Reduction on the peak accelerations is observed as well, although slight increases are found for some cases. Therefore, it can be concluded that the designed control systems based on the VDNS algorithm are effective in reducing the responses of the building under earthquakes, and the performance is especially good for the floor displacement and interstory drift.

Both control systems are robust to the changes of the building's properties. Although the controllers are designed based on the pre-earthquake model of the building, significant response reductions are achieved in the post-earthquake structure as well. Increases of the maximum base shear under all four earthquake excitations are observed. The reason might be the relative lower stiffness of the post-earthquake structure after strong earthquake motion. When the same control force is applied by the control algorithm, the whole structure becomes relatively stiffer for the post-earthquake model.

Generally, the active control system produces slightly better results than the semi-active system, while significant reductions by the semi-active system are observed in the normed interstory drift, as compared to the active system. In addition, the semi-active system requires significantly less power than the active controller. The designed control

systems produce better results in the floor displacement and interstory drift than the provided sample controller, and have comparable performance in the acceleration response, demonstrating again the effectiveness of the control algorithm and the designed systems.

CHAPTER 5. SUMMARY

This thesis studied the application of the viscous damping and negative stiffness (VDNS) control algorithm to reduce the responses of civil buildings under earthquakes. VDNS is a very simple algorithm, as compared to other control strategies that require the designers to have deep understanding in modern control theory. It provides an effective option for the semi-active control of the seismically excited buildings.

The H2/LQG control method is one of the most widely used control strategies in structural control and has been shown to be effective in many applications. The H2/LQG method was provided in detail in Chapter 2. In this method, weighting matrices **Q** and **R** are specified for a performance index (or cost function) *J*. An optimal gain matrix **K** is then calculated to minimize the performance index, by solving the algebraic Riccati equation. Herein the performance index *J* is a mathematical function involving the regulated responses and control inputs, without certain physical meaning. Therefore, the controller is designed in a mathematical perspective. In addition, for the designers, it is usually unclear how the gain matrix **K** is derived by the algebraic Riccati equation, and why the derived **K** makes the performance index *J* minimum. **K** is usually solved directly by MATLAB in the control system design.

The pseudo negative stiffness (PNS) algorithm proposed by Iemura et al. gives a control force with simple form, which consists of only a viscous damping force and a negative stiffness force. Iemura et al. indicated that the PNS-controlled damper could reduce the seismic responses of the cable-stayed bridges, because the PNS loop reduced the total force of the damper force and the existing-member stiffness force while keeping large area inside the hysteretic loop. In addition, they observed that the LQR controller could also produce the pseudo negative stiffness hysteretic loops, and they believed that the

produced pseudo negative stiffness hysteretic loops should be one of the reasons that make the LQG controller effective.

The viscous damping and negative stiffness (VDNS) control algorithm was proposed by Weber et al. for the mitigation of stay cable vibrations. The idea of the VDNS algorithm is to mitigate the stay cable vibrations by increasing the cable damping. The control force produced by this algorithm has the same form as that of PNS algorithm. To apply the VDNS algorithm to the response control of buildings, a numerical example was provided in Chapter 3 to demonstrate the procedure. In the example, the results of the designed controllers based on the VDNS strategy were better than those of the clipped optimal controllers. Furthermore, the VDNS algorithm only requires the measurements at the locations of control devices. Therefore, the control system can be designed decentralized.

A 20-story linear benchmark building was used to evaluate the performance of the VDNS algorithm. An active control system using hydraulic actuators and a semi-active system using MR dampers were designed based on the VDNS algorithm. Both designed control systems were effective in reducing the seismic responses of the building, especially the relative displacements and interstory drifts. All the normed responses and the peak relative displacement and interstory drift were reduced by the control systems. The results of the semi-active system were comparable to those of the active control. In addition, the control systems were observed to be robust to the changes of the building's properties.

The biggest advantage of the VDNS algorithm is its simplicity. Firstly, the controller design process is simple. Only two control parameters are involved. The control parameters are selected to increase the structural damping, which is more intuitive to the designers. Secondly, the resulted control force is simple, which could reduce the calculation time of the processing units. Furthermore, the control system can be implemented decentralized. It eliminates the long cables between different floors, reduces the communication time and decreases the uncertainties in the communication.

Nevertheless, the VDNS also has some drawbacks. During the design of the control system, some assumptions are made to simplify the problem. For example, the effects of higher modes on the response of the buildings are not considered in the determination of control parameters. In addition, more sensors, control devices and processing units are needed for large scale buildings.

5.1. Future Work

Both centralized and decentralized approaches have pros and cons regarding robustness to failure. With a centralized controller, one can switch from a controller that uses full sensors to a controller that uses fewer sensors when a failure is detected. So it is could be robust with proper provisions. On the other hand, for the decentralized controller, the entire control system can be divided into multiple subsystems. If one subsystem fails, the other subsystems might be able to compensate accordingly, and help to avoid the failure of the whole system. The control system based on the VDNS algorithm can be implemented decentralized. It would be worthwhile to study the fault tolerance of the control system.

The VDNS control strategy has been demonstrated effective in the numerical examples. It should also be studied experimentally.

The buildings studied in this thesis were assumed to remain in the linear region, but buildings could become nonlinear in strong earthquakes. Methods of controlling the nonlinear buildings should be investigated.

During the design of the VDNS controller, the information of the earthquake excitations are not required, i.e., the controller is designed to work for all earthquakes generally. Future investigation could analyze and compare the performances of the controller for different earthquakes.

LIST OF REFERENCES

[1] Yao, J.T.P. (1972). "Concept of Structural Control," *Journal of the Structural Division, ASCE*, Vol. 98, pp. 1567–1574.

[2] Spencer Jr., B.F. and Nagarajaiah, S. (2003). "State of the Art of Structural Control," *Journal of Structural Engineering, ASCE,* Vol. 129, No. 7, pp. 845–856.

[3] Yi, F. and Dyke, S.J. (2000). "Structural Control Systems: Performance Assessment," *Proc. of the 2000 American Control Conference,* Chicago, Illinois, June 28-30.

[4] Jansen, L.M., (2000), *Response Modification of Buildings and Bridges: Comparative Studies in Seismic Control*. Master Thesis. Washington University, St. Louis, Missouri.

[5] Housner, G.W., Bergman, L.A., Caughey, T.K., Chassiakos, A.G., Claus, R.O., Masri, S.F., Skelton, R.E., Soong, T.T., Spencer, B.F., and. Yao, J.T.P. (1997). "Structural Control: Past, Present, and Future," *Journal of Engineering Mechanics*, Vol. 123, No. 9, pp. 897–971.

[6] Narasimhan, S., Nagarajaiah, S., Johnson, E.A. and Gavin, H.P. (2006), "Smart Base-Isolated Benchmark Building. Part I: Problem Definition," *Structural Control Health Monitoring,* Vol. 13, pp. 573–588.

[7] Spencer, Jr. B.F., Dyke, S.J., and Deoskar, H.S. (1998). "Benchmark Problems in Structural Control: Part I – Active Mass Driver System," *Earthquake Engineering and Structural Dynamics: Special Issue on the Benchmark Structural Control Comparison,* Vol. 27, No. 11, pp. 1127–1139.

[8] Dyke, S.J., Spencer Jr., B.F., Quast, P., Kaspari Jr., D.C., and Sain, M.K. (1996). "Implementation of an AMD Using Acceleration Feedback Control," *Microcomputers in Civil Engineering*, Vol. 11, pp. 305–323.

[9] Dyke, S.J., Spencer Jr., B.F., Quast, P., Sain, M.K., Kaspari Jr., D.C. and Soong, T.T. (1994). "Experimental Verification of Acceleration Feedback Control Strategies for an Active Tendon System," *National Center for Earthquake Engineering Research,* Tech. Report NCEER-94-0024, Buffalo, N.Y.

[10] Dyke, S.J., Spencer, Jr., B.F., Quast, P. Sain, M.K., Kaspari, Jr. D.C. and Soong, T.T. (1996), "Acceleration Feedback Control of MDOF Structures" *Journal of Engineering Mechanics,* Vol. 122, No. 9, pp. 907-918.

[11] Leitmann, G. (1994). "Semiactive Control for Vibration Attenuation," *Journal of Intelligent Material Systems and Structures,* Vol. 5, pp. 841-846.

[12] McClamroch, N.H. and Gavin, H.P. (1995). "Closed Loop Structural Control Using Electrorheological Dampers," *Proc. of the Amer. Ctrl. Conf.,* Seattle, Washington, pp. 4173-4177.

[13] Jansen L.M. and Dyke S.J. (2000). "Semi-Active Control Strategies for the MR Damper: A Comparative Study" *Journal of Engineering Mechanics,* Vol. 126, No. 8, pp. 795–803.

[14] Dupont, P., Kasturi, P., and Stokes, A. (1997). "Semi-Active Control of Friction Dampers" *Journal of Sound and Vibration,* Vol. 202, No. 2, pp. 203-218.

[15] Becker, J. and Gaul, L. (2007). "Semi-Active Control of Adaptive Friction Dampers for Structural Vibration Control," *Proceedings of the IMAC-XXV: A Conference & Exposition on Structural Dynamics,* Orlando, Florida.

[16] Lane, J.S. and Ferri, A.A. (1992). "Optimal Control of a Semi-Active, Frictionally Damped Joint," *Proceedings of American Control Conference,* Chicago, Illinois, June 24-26, pp. 2754-2759.

[17] Wang, K.W., Kim, Y.S., and Shea, D.B. (1994). "Structural Vibration Control via Electrorheological –Fluid-Based Actuators with Adaptive Viscous and Frictional Damping," *Journal of Sound and Vibraion,* Vol. 177, No. 2, pp. 227-237.

[18] Dyke, S.J. and Spencer Jr. B.F. (1997). "A Comparison of Semi-Active Control Strategies for the MR Damper," *Proc. of the IASTED Intl. Conf. on Intelligent Info. Systems,* Bahamas, December 8-10, pp. 580–584.

[19] Dyke, S.J., B.F. Spencer, Jr., M.K. Sain, and Carlson, J.D. (1996). "Seismic Response Reduction Using Magnetorheological Dampers." *Proc. of the IFAC World Congress,* San Francisco, California, Vol. L, pp. 145-150.

[20] Dyke, S.J., Spencer Jr., B.F., Sain, M.K. and Carlson, J.D. (1996). "Modeling and Control of Magnetorheological Dampers for Seismic Response Reduction," *Smart Materials and Structures,* Vol. 5, pp. 565-575.

[21] Dyke, S.J., Spencer Jr., B.F., Sain, M.K., and Carlson, J.D. (1996). "Experimental Verification of Semi-Active Structural Control Strategies Using Acceleration Feedback," *Proc. of the 3rd Intl. Conf. on Motion and Vibr. Control*, Chiba, Japan, September, Vol. 3, pp. 291-296.

[22] Spencer Jr., B.F., Dyke, S.J., Sain, M.K., and Carlson, J.D., (1997). "Phenomenological Model for Magnetorheological Dampers," *Journal of Engineering Mechanics, ASCE*, Vol. 123, No. 3, pp. 230-238.

[23] Yu, W. (2009). *Recent Advances in Intelligent Control Systems*. Berlin: Springer, pp 4-6.

[24] Sodeyama, H., Suzuki, K., and Katsuaki, S. (2004). "Development of Large Capacity Semi-Active Seismic Damper Using Magneto-Rheological Fluid", *Journal of Pressure Vessel Technology*, Vol. 126, pp. 105-109.

[25] Yi, F., Dyke, S. J., Caicedo, J. M., and Carlson, J. D. (2001). "Experimental Verification of Multi-Input Seismic Control Strategies for Smart Dampers." *Journal of Engineering Mechanics, ASCE*, Vol. 127, No. 11, pp. 1152–1164.

[26] Yoshida, O., Dyke, S. J., Giacosa, L. M., and Truman, K. Z. (2002). "An Experimental Study on Seismic Response Control of Asymmetric Buildings Using MR Dampers," *Proeedings. of The 11th Japan Earthquake Engineering Symposium*, Tokyo, Japan, November 20–22.

[27] Yoshida, O., (2003), *Torsionally Coupled Response Control of Earthquake Excited Asymmetric Buildings: Development and Application of Effective Control Systems Using Smart Dampers*. Doctoral Dissertation. Washington University, St. Louis, Missouri.

[28] Yoshida, O. and Dyke, S.J. (2004), "Seismic Control of a Nonlinear Benchmark Building Using Smart Dampers" *Journal of Engineering Mechanics*, Vol. 130, No. 4, pp. 386-392.

[29] Iemura, H. and Pradono, M. H. (2002). "Passive and Semi-Active Seismic Response Control of a Cable-Stayed Bridge," *Journal of Structural Control*, Vol. 9, pp. 189-204.

[30] Iemura, H. and Pradono, M. H. (2003). "Application of Pseudo-Negative Stiffness Control to the Benchmark Cable-Stayed Bridge," *Journal of Structural Control*, Vol. 10, pp 187-203.

[31] Iemura, H. and Pradono, M. H. (2004). "Pseudo Negative Stiffness Dampers for Earthquake Response Control of Cable-Stayed Bridges," *Proceedings of 13th World Conference on Earthquake Engineering*, Vancouver, B.C., Canada, August 1-6.

[32] Iemura, H. and Pradono, M. H. (2005). "Simple Algorithm for Semi-Active Seismic Response Control of Cable-Stayed Bridges," *Earthquake Engineering. Structural Dynamics*, Vol. 34, pp 409-423.

[33] Wu, B., Shi, P. and Ou, J. (2011). "Seismic Performance of Structures Incorporating Magnetorheological Dampers with Pseudo-Negative Stiffness," *Structural Control Health Monitoring*.

[34] Ou, J. and Li, H. (2009). "Design Approaches for Active, Semi-Active and Passive Control Systems Based on Analysis of Characteristics of Active Control Force" *Earthquake Engineering and Engineering Vibration*, Vol. 8, No. 4, pp. 493-506.

[35] Ou, J. and Li, H. (2010). "Analysis of Capability for Semi-Active or Passive Damping Systems to Achieve the Performance of Active Control Systems," *Strucural. Control Health Monioring.*, Vol. 17, pp. 778-794.

[36] Weber, F. and Boston, C. (2011). "Clipped Viscous Damping with Negative Stiffness for Semi-Active Cable Damping," *Smart Materials and Structures*, Vol. 20.

[37] Weber, F., Feltrin, G., Huth, O. (2006). *Guidelines for Structural Control*, SAMCO Final Report 2006.

[38] Liang, Z., Lee, G.C., Dargush, G.F., Song, J. (2012). *Structural Damping: Applications in Seismic Response Modification*. Boca Raton, FL: CRC Press.

[39] Spencer Jr., B.F., Christenson, R.E., and Dyke, S.J. (1998). "Next Generation Benchmark Control Problem for Seismically Excited Buildings," *Proceedings of the Second World Conference on Structural Control*, Wiley, Kyoto, Japan, June 29-July 2.